

An open access, peer-reviewed, international journal of science. Biannual (June & December). ISSN 2147-1630
| e- ISSN 2146-586X. Publisher: Adiyaman University.

Publication language: English (with Turkish title and abstract)

Issue published date: 28.06.2024

Privilege owner: On Behalf of the Rectorate of Adiyaman University, Prof. Dr. Mehmet KELLEŞ (Rector)

Web site: EN: <https://dergipark.org.tr/en/pub/adyujsci>
TR: <https://dergipark.org.tr/tr/pub/adyujsci>

EDITORIAL BOARD

Editor in Chief : Selcen YÜKSEL PERKTAŞ, Ph.D.

Co-Editor : Ali Osman AYAŞ, Ph.D.

Editors

Biology : Serdar SÖNMEZ, Ph.D.

: Ertan YOLOĞLU, Ph.D.

Chemistry : Cumhuri KIRILMIŞ, Ph.D.

: Gökhan ELMACI, Ph.D.

Mathematics : Serbay DURAN, Ph.D.

: Merve AVCI ARDIÇ, Ph.D.

Physics : Salim ÇERÇİ, Ph.D.

: Özge ERKEN, Ph.D.

Language Editors : Münevver AKBAŞ

Section Editors

Biology:

Aydın AKBUDAK, Ph.D.

Bahadır AKMAN, Ph.D.

Birgül ÖZCAN, Ph.D.

Deniz AYAS, Ph.D.

Hasan YILDIZ, Ph.D.

Olga SAK, Ph.D.

Özkan ASLANTAŞ, Ph.D.

Si Hong PARK, Ph.D.

Süphan KARAYTUĞ, Ph.D.

Chemistry:

Sezgin BAKIRDERE, Ph.D.

H. Mehmet KAYILI, Ph.D.

Önder METİN, Ph.D.

Zeynel SEFEROĞLU, Ph.D.

Lokman UZUN, Ph.D.

Mathematics:

Ramazan AKGÜN, Ph.D.

Murat CANDAN, Ph.D.

Feyza Esra ERDOĞAN, Ph.D.

Mehmet Onur FEN, Ph.D.

Öznur GÖLBAŞI, Ph.D.

Mehmet GÜLBAHAR, Ph.D.

Bilge İNAN, Ph.D.

Eylem GÜZEL KARPUZ, Ph.D.

Aynur KESKİN KAYMAKCI, Ph.D.

Mustafa Çağatay KORKMAZ, Ph.D.

James F. PETERS, Ph.D.

Tahsin ÖNER, Ph.D.

Physics:

Ahmet EKİCİBİL, Ph.D.

Didar DOBUR, Ph.D.

Daniel GREEN, Ph.D.

Faruk KARADAĞ, Ph.D.

Hakan ÖZTÜRK, Ph.D.

Kristina RUSIMOVA, Ph.D.

Latife ŞAHİN YALÇIN, Ph.D.

Mustafa GÜNEŞ, Ph.D.

Paolo GUNNELLINI, Ph.D.

Technical Contact: Serdar SÖNMEZ, Ph.D., ssonmez@adiyaman.edu.tr, sonmezserdar@gmail.com



The articles published in this journal are licensed under a Creative Commons Attribution- NonCommercial-ShareAlike 4.0 International License.

Table of Contents (İçindekiler)
Volume (Cilt): 14 Number (Sayı): 1 June (Haziran) 2024

CHEMISTRY:

- Effect of co-agent type on curing kinetics of vinyl-methyl siloxane and phenyl-vinyl-methyl siloxane elastomers**
Ko-ajan tipinin vinil-metil siloksan ve fenil-vinil-metil siloksan elastomerlerinin kür kinetiğine etkisi 1-16
Davut AKSÜT, Elif KAYMAZLAR, Murat ŞEN
-
-

MATHEMATICS:

- On New Spinor Sequences of Jacobsthal and Jacobsthal-Lucas Quaternions**
Jacobsthal ve Jacobsthal-Lucas Kuaterniyonlarının Yeni Spinor Dizileri Üzerine 17-38
Tülay ERİŞİR, Mehmet Ali GÜNGÖR

- Existence and Uniqueness of Almost Periodic Solutions to Time Delay Differential Equations**
Zaman Gecikmeli Diferansiyel Denklemlerin Yaklaşık Periyodik Çözümlerinin Varlığı ve Tekliği 39-50
Münevver TUZ
-
-

PHYSICS:

- Structural and Luminescence Characterization of LiAlO₂ Ceramics Synthesized by Sol-Gel Technique**
Sol-Jel Tekniği ile Sentezlenen LiAlO₂ Seramiklerinin Yapısal ve Lüminesans Karakterizasyonu 51-63
Volkan ALTUNAL



Effect of co-agent type on curing kinetics of vinyl-methyl siloxane and phenyl-vinyl-methyl siloxane elastomers

Davut AKSÜT^{1, *}, Elif KAYMAZLAR², Murat ŞEN³

¹*Hacettepe University, Faculty of Science, Department of Chemistry, 06800, Ankara, Turkey
davut.aksut@hacettepe.edu.tr, ORCID: 0000-0003-0954-07027*

²*Ondokuz Mayıs University, Faculty of Arts and Sciences, Department of Chemistry, 55139, Samsun, Turkey*

elif.kaymazlar@omu.edu.tr, ORCID: 0000-0001-8960-9610

³*Hacettepe University, Faculty of Science, Department of Chemistry, 06800, Ankara, Turkey
msen@hacettepe.edu.tr, ORCID: 0000-0001-8640-680X*

Received: 25.01.2024

Accepted: 07.06.2024

Available online: 28.06.2024

Abstract

In this study, Type I co-agents Zinc Acrylate (ZDA), Zinc Methacrylate (ZDMA) and Type II co-agents Triallyloxy-1,3,5-triazine (TAC) and 1,3,5-triallyl-1,3,5-triazine (TAIC) on the curing kinetics of vinyl methyl polysiloxane (VMQ) and phenyl vinyl methyl polysiloxane (PVMQ) elastomers was examined. Cure rate constant (k), reaction degree (n), and activation energy (E_a) values were evaluated according to the 1st and nth cure kinetics, using the data of the cure curves obtained from the rheological analyses performed with the moving die rheometer at different temperatures. It was determined that the type of co-agent used in the preparation of the elastomer had a positive effect on the cure rate and effective cross-link formation. In addition, the effect of both

* Corresponding author: Davut Aksüt, Hacettepe University, Faculty of Science, Department of Chemistry, 06800, Ankara, Turkey Email: davut.aksut@hacettepe.edu.tr



the molecular structure of the co-agent used and the type of silicone elastomer on the cure reaction was explained. Since activation energies were calculated using the entire cure curve in the n^{th} degree cure kinetics, higher activation energy values were obtained compared to the 1st-degree cure kinetics. While the use of co-agents has been shown to affect the curing behavior and rheology of silicone elastomers, it is clear that the elastomer components and type of coagent will affect the performance of the final product.

Keywords: Activation energy; Co-agent; Peroxide curing; Silicone elastomer.

Ko-ajan tipinin vinil-metil siloksan ve fenil-vinil-metil siloksan elastomerlerinin kür kinetiğine etkisi

Öz

Bu çalışmada Tip I ko-ajanlar Çinko Akrilat (ZDA), Çinko Metakrilat (ZDMA) ve Tip II ko-ajanlar Trietiloksi-1,3,5-triazin (TAC) ve 1,3,5-trialil-1,3,5-triazinin (TAIC), vinil metil polisiloksan (VMQ) ve fenil vinil metil polisiloksan (PVMQ) elastomerlerinin kürlenme kinetiği üzerindeki etkisi incelenmiştir. Kürleşme hızı sabiti (k), reaksiyon derecesi (n) ve aktivasyon enerjisi (E_a) değerleri, hareketli kalıp Reometresi ile farklı sıcaklıklarda gerçekleştirilen reolojik analizlerden elde edilen kürlenme eğrilerinin verileri kullanılarak 1. ve n . kür kinetiğine göre değerlendirildi. Elastomerin hazırlanmasında kullanılan ko-ajan türünün kürleşme hızına ve etkili çapraz bağ oluşumuna olumlu etkisi olduğu belirlendi. Ayrıca hem kullanılan ko-ajanın moleküler yapısının hem de silikon elastomer tipinin kür reaksiyonuna etkilediği tesbit edilmiştir. n . derece kür kinetiğinde aktivasyon enerjileri kür eğrisinin tamamı kullanılarak hesaplandığından 1. derece kür kinetiğine göre daha yüksek aktivasyon enerjisi değerleri elde edilmiştir. Yardımcı ajanların kullanımının silikon elastomerlerin kür davranışını ve reolojisini üzerindeki etkisi görülmüştür. Elastomer bileşenlerinin ve ko-ajan tipinin nihai ürünün performansını etkileyeceği açıktır.

Anahtar Kelimeler: Aktivasyon enerjisi; Ko-ajan; Peroksit kürleme, Silikon elastomer.

1. Introduction

Silicone elastomers have been used in many applications because of their chain flexibility, and thermal resistance and maintain their physical properties at a wide temperature range. Siloxane bonds (Si-O-Si) form the skeleton of the silicone structure. Silicone structures with different properties can be obtained by bonding other organic groups to the silicon atom [1]. As a result of the cross-linking of the elastomers, their physical properties and dynamic performances are significantly increased [2]. The strength and quantity of the cross-links affect the stiffness,

mechanical properties, and network structure of the elastomer. Usually, organic peroxides are used for crosslinking of silicone elastomers. Organic peroxides are the structures formed by bonding at least two oxygen atoms bonded to an organic group. The peroxide decomposes with the heat to form free radicals, forming the active group on the polymer chain. Crosslinking occurs with the interaction of the active parts formed on the polymer chains. The chemical structure of the organic group attached to the oxygens in peroxides allows the peroxide to be classified as dialkyl, diacyl, peroxyketal, and peroxyester. Some peroxides in these peroxide classes, and often used with silicone elastomers have advantages and disadvantages.

Peroxyketals react more quickly due to their low half-life. Peroxyketals give a high curing reaction at low temperatures compared to diacyl peroxides. However, since peroxyketals contain both weak and strong free radicals, they show less efficient cross-linking than dialkyls [3]. Diacyl peroxides, on the other hand, form highly active free radicals when they decompose. However, they are preferred in processes that require little crosslinking because they require a high curing temperature and have a long half-life [4]. It is frequently used in co-agents in systems where silicone elastomers are cured by peroxide curing. Co-agents or accelerators are important additives as they affect the activity of crosslinking agents and the amount of crosslinking [5]. They also change processing parameters such as cure rate and cure time [6]. Co-agents used with peroxide are classified as Type I and Type II based on their contributions to cure. Type I co-agents increase both the rate and state of cure. Type II co-agents form less reactive radicals and contribute only to the state of cure [7]. Type I co-agents have two functional groups, and Type II has three functional groups. Type I accelerators are generally polar, multifunctional, and have low molecular weight. Type I accelerators contain acrylates, methacrylates, methacrylate esters, and dimelamides in their structure. Type II accelerators are radicals with lower activity and only increase the number of crosslinks. Type II accelerators contain allyl groups, cyanurate, isocyanurate, and phthalates.

Experimental investigations of the cure and rheology of elastomers are crucial for understanding how to achieve the highest quality components in manufacturing processes. However, this empirical approach is often complex and time-consuming. Numerical modeling and simulations offer a more cost-effective alternative, allowing for iterative studies without the need for extensive in situ trials. In addition, experimental research on the curing and rheology of elastomers can give us information about the components that the highest quality product will need, the production method, and factors affecting the performance of the end product, etc. in a production process [8].

In this study, we have investigated the effect of various co-agents on the curing kinetics of different polysiloxane elastomers at different temperatures. The impact of different co-agent types on curing was examined with 1st and nth cure kinetics models. The investigation into the effects of co-agents on the curing kinetics and cure parameters of polysiloxane elastomer reveals that, although co-agents significantly influence the curing behavior and rheology of silicone elastomers, the performance of the final product is also heavily dependent on the elastomer components and the type of manufacturing process used.

2. Materials and Methods

2.1. Materials

Phenyl vinyl methyl silicone (PVMQ) was purchased from Shin-Etsu Chemical Co. Ltd. (Tokyo, Japan). Vinyl methyl silicone (VMQ) was purchased from Wacker Co. Ltd. (USA). Co-agents, triallyl cyanurate (TAC), triallyl isocyanurate (TAIC), zinc diacrylate (ZDA), and zinc dimethacrylate (ZDMA) were obtained from Sigma-Aldrich. As crosslinker, 2,5-dimethyl-2,5-di(tertiary-butylperoxy) hexane (DBPH) with product code trigonox 101-45S and peroxide content of 44-46% was obtained from Akzo Nobel (Netherlands). The mold release agent (MRA) used to remove elastomers from vulcanization molds was purchased from SolPro Co.Ltd. (Türkiye).

2.2. Preparation of compounds and vulcanizates

In the formulations specified in **Table 1**, silicone elastomers have been prepared in the Thermo HAAKE Rheomix Mixer system at 25 °C for 20 minutes at a rate of 50 rpm. Cure characteristics at these rubber blends (etc: scorch time t_{2s} , optimum cure time t_{90} , and torque increments ΔM) were determined according to ASTM D 5289 using Alpha 2000B Moving Die Rheometer (MDR) at five different temperatures 170, 175, 180, 185 and 190 °C for 20 minutes.

Table 1. Formulations of the compounds.

<i>Blends Code</i>	<i>Components, phr*</i>							
	<i>VMQ</i>	<i>PVMQ</i>	<i>DPBH</i>	<i>TAC</i>	<i>TAIC</i>	<i>ZDA</i>	<i>ZDMA</i>	<i>MRA**</i>
VMQ	100	-	0.8	-	-	-	-	1.25
VMQ-TAC	100	-	0.8	0.5	-	-	-	1.25
VMQ-TAIC	100	-	0.8	-	0.5	-	-	1.25
VMQ-ZDA	100	-	0.8	-	-	0.5	-	1.25
VMQ-ZDMA	100	-	0.8	-	-	-	0.5	1.25
PVMQ	-	100	0.8	-	-	-	-	1.25
PVMQ-TAC	-	100	0.8	0.5	-	-	-	1.25
PVMQ-TAIC	-	100	0.8	-	0.5	-	-	1.25
PVMQ-ZDA	-	100	0.8	-	-	0.5	-	1.25
PVMQ-ZDMA	-	100	0.8	-	-	-	0.5	1.25

*phr, Parts per Hundred Rubber, **MRA, Mould release agent

2.3. Characterization

The rheological analysis of the silicone blends has been performed using Alpha Technologies MDR 2000B rheometer according to ASTM D5289. The mechanical properties of the blends have been investigated using a Zwick/Z010 Universal Testing Machine according to ASTM D412 with a crosshead speed of 100 mm/min.

3. Theoretical Background

3.1. 1st Order Kinetic Model

Cure Rate Index (CRI) which is related to the rate of vulcanization was calculated using Equation 1 [9].

$$\text{CRI} = 100 / (t_{90} - t_{s2}) \quad (1)$$

The cure rate content and activation energy of silicone elastomers were calculated according to 1st order kinetic model. The state of cure (α) values were calculated by evaluating cure curves of VMQ and PVMQ elastomers at four different temperatures using equation 2 [10].

$$\alpha(t) = (M_t - M_H) / (M_H - M_L) \quad (2)$$

Where M_H is the maximum torque, M_L is the minimum torque and M_t is the torque at the time t . k values were calculated according to 1st order kinetic model using Equation 3 by evaluating the area between $\alpha=0.25-0.45$ in the cure curve.

$$\ln(\alpha) = k(T) \cdot t \quad (3)$$

Activation energies of elastomers have been calculated with k values obtained at different temperatures using the Arrhenius equation.

$$k = k_0 \exp\left(-\frac{E_a}{RT}\right) \quad (4)$$

Where E_a is the activation energy, R is the universal gas constant and T is the absolute temperature.

3.2. nth order kinetic model

The second method for calculating k , E_a , and reaction order (n) is the n^{th} -order kinetic model. The state of cure-time curves was evaluated using a scientific program according to Equation 5 to obtain k and n values.

$$\alpha = k[(t - t_s)]^n / (1 + k[(t - t_s)]^n) \quad (5)$$

Where t_s is scorch time, activation energies of elastomers have been calculated using Equation 4.

4. Results and Discussion

4.1. Cure characteristics of VMQ & PVMQ at different temperatures

Silicone elastomers are prepared according to the recipes given in **Table 1**. They were cured at 170, 175, 180, 185, and 190 °C. The cure curves of VMQ and P VMQ elastomers without co-agents at 5 different temperatures are given in **Figures 1-a** and **1-b**.

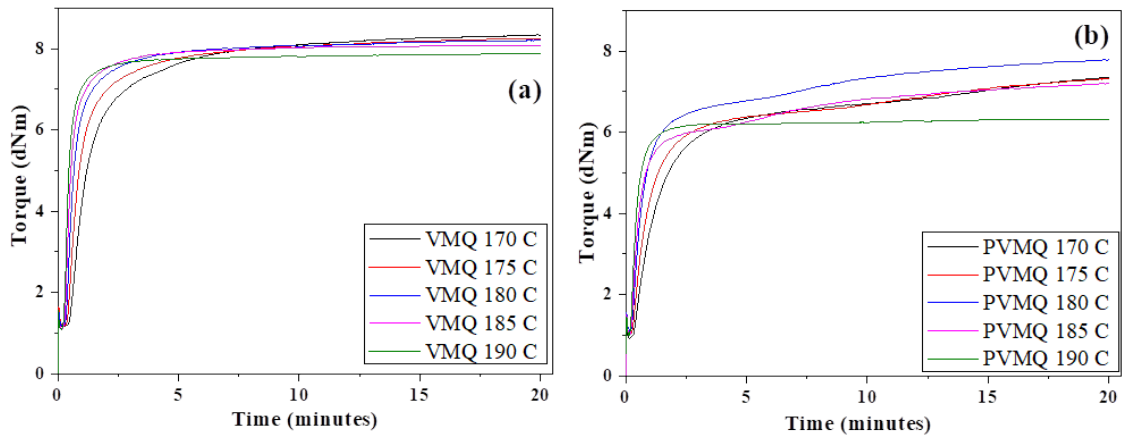


Figure 1. The cure curves of VMQ and PVMQ compounds.

The curing characteristic parameters of PVMQ and VMQ elastomers at different temperatures are presented in **Table 2** and **Table 3**, respectively.

The curing curves give valuable information into the curing behavior of elastomers. Tables 2 and 3 include parameters such as scorch time (t_{s2}), optimum cure time (t_{90}), and the cure rate index (CRI) which is a parameter that indicates the rate of the curing reaction. It is indicative of the curing performance and efficiency of the compounds. In addition, Δ_{torque} , which is the degree of cure is the difference between the minimum torque and the maximum torque. The torque difference in an MDR test is proposed to be theoretically linked to the shear dynamic modulus, and this modulus is indirectly associated with the total crosslink density in rubber compounds [16].

Table 2. Cure characteristic parameters of PVMQ.

Temperature	Cure Parameter	PVMQ	PVMQ-TAC	PVMQ-TAIC	PVMQ-ZDA	PVMQ-ZDMA
170 ° C	M_L (dNm)	0.92±0.02	0.95±0.05	0.96±0.03	1.21±0.02	1.08±0.08
	M_H (dNm)	7.35±0.98	12.19±1.22	12.48±1.01	11.07±0.87	11.23±0.99
	ts_2 (min)	0.79±0.02	0.77±0.03	0.68±0.03	0.44±0.04	0.65±0.34
	t_{90} (min)	10.03±0.99	3.65±0.31	3.60±0.38	3.00±0.02	3.90±0.74
	CRI(min^{-1})	10.8±0.9	34.7±2.6	34.3±4.3	39.1±2.8	30.8±1.6
175 ° C	M_L (dNm)	1.04±0.02	0.99±0.01	0.92±0.08	1.23±0.02	1.14±0.08
	M_H (dNm)	7.33±0.67	12.06±0.99	11.98±0.99	11.00±0.94	10.42±0.54
	ts_2 (min)	0.63±0.06	0.60±0.05	0.53±0.08	0.36±0.06	0.55±0.04
	t_{90} (min)	10.37±0.95	2.53±0.21	2.51±0.87	1.63±0.07	2.74±0.17
	CRI(min^{-1})	10.3±0.8	51.8±3.5	50.5±4.1	78.7±0.7	45.7±2.3
180 ° C	M_L (dNm)	1.11±0.02	0.99±0.04	0.98±0.08	1.10±0.65	1.19±0.21
	M_H (dNm)	7.79±0.79	12.41±0.95	12.18±1.00	10.40±0.09	10.61±0.84
	ts_2 (min)	0.48±0.03	0.46±0.02	0.43±0.03	0.31±0.02	0.43±0.03
	t_{90} (min)	7.94±0.98	1.81±0.32	1.77±0.87	1.19±0.09	1.86±0.06
	CRI(min^{-1})	13.4±1.2	74.1±6.5	74.6±6.9	113.6±13.2	69.9±4.3
185 ° C	M_L (dNm)	1.00±0.02	0.96±0.03	1.07±0.03	1.17±0.07	1.22±0.85
	M_H (dNm)	7.21±0.95	12.19±1.01	12.09±0.99	10.02±0.86	10.50±0.08
	ts_2 (min)	0.41±0.04	0.38±0.05	0.36±0.04	0.28±0.03	0.36±0.04
	t_{90} (min)	7.35±0.76	1.27±0.21	1.23±0.21	0.92±0.07	1.34±0.03
	CRI(min^{-1})	14.4±1.2	112.4±9.8	114.9±13.2	156.3±16.2	102.0±8.7
190 ° C	M_L (dNm)	1.00±0.02	1.04±0.01	0.94±0.07	1.30±0.03	1.18±0.05
	M_H (dNm)	6.33±0.36	12.32±0.58	11.27±0.99	10.42±0.42	9.76±0.96
	ts_2 (min)	0.35±0.01	0.33±0.02	0.31±0.02	0.24±0.03	0.32±0.02
	t_{90} (min)	1.11±0.32	0.96±0.08	0.91±0.07	0.70±0.04	1.01±0.01
	CRI(min^{-1})	131.6±11.4	158.7±13.2	166.7±14.6	217.4±15.1	144.9±9.5

Table 3. Cure characteristic parameters of VMQ.

Temperature	Cure Parameter	VMQ	VMQ-TAC	VMQ-TAIC	VMQ-ZDA	VMQ-ZDMA
170 ° C	M_L (dNm)	1.15±0.05	1.11±0.08	1.20±0.22	1.34±0.87	1.38±0.07
	M_H (dNm)	8.35±0.25	16.04±0.14	15.26±0.90	11.36±1.24	11.18±0.93
	ts_2 (min)	0.80±0.01	0.74±0.07	0.72±0.08	0.46±0.01	0.67±0.02
	t_{90} (min)	4.96±0.09	3.12±0.25	2.91±0.12	1.64±0.24	3.10±0.04
	CRI(min^{-1})	24.0±0.2	42.0±2.1	45.7±2.3	84.7±6.5	41.2±1.4
175 ° C	M_L (dNm)	1.17±0.11	1.14±0.04	1.18±0.41	1.39±0.08	1.32±0.08
	M_H (dNm)	8.26±0.32	15.70±1.02	15.02±0.51	11.01±0.99	10.75±0.87
	ts_2 (min)	0.62±0.02	0.57±0.03	0.55±0.02	0.39±0.01	0.54±0.04
	t_{90} (min)	3.68±0.08	2.15±0.32	1.96±0.11	1.14±0.02	2.22±0.87
	CRI(min^{-1})	32.7±1.9	63.3±5.8	70.9±2.3	133.3±9.8	59.5±3.8
180 ° C	M_L (dNm)	1.17±0.35	1.13±0.08	1.15±0.30	1.34±0.08	1.31±0.02
	M_H (dNm)	8.22±0.25	15.58±1.25	14.79±1.01	10.89±0.87	10.82±0.98
	ts_2 (min)	0.49±0.02	0.46±0.01	0.44±0.01	0.34±0.01	0.44±0.02
	t_{90} (min)	2.44±0.23	1.68±0.11	2.09±0.02	0.94±0.02	1.55±0.07
	CRI(min^{-1})	51.3±2.5	81.9±4.2	60.6±1.9	166.6±12.3	90.1±5.6
185 ° C	M_L (dNm)	1.12±0.11	1.12±0.09	1.09±0.01	1.30±0.03	1.28±0.08
	M_H (dNm)	8.10±0.90	15.40±1.42	14.52±0.98	10.55±0.57	10.58±0.98
	ts_2 (min)	0.40±0.01	0.39±0.02	0.39±0.01	0.30±0.01	0.36±0.04
	t_{90} (min)	1.74±0.02	1.21±0.08	1.09±0.02	0.70±0.03	1.13±0.01
	CRI(min^{-1})	74.6±3.6	121.9±8.9	142.8±7.5	250.0±18.7	129.9±8.9
190 ° C	M_L (dNm)	1.09±0.02	1.08±0.01	1.06±0.02	1.28±0.18	1.27±0.03
	M_H (dNm)	7.89±0.94	14.82±0.21	14.33±0.97	10.48±0.54	10.41±0.99
	ts_2 (min)	0.35±0.03	0.34±0.02	0.33±0.02	0.26±0.01	0.32±0.04
	t_{90} (min)	1.17±0.08	0.86±0.04	0.83±0.09	0.55±0.02	0.87±0.09
	CRI(min^{-1})	121.9±8.9	192.3±9.3	200±15.68	344.8±18.9	181.8±7.4

Analyzing the curing curves of these compounds, a noticeable trend emerged – the delta torque value rose with the use of co-agents. Moreover, this increase was more pronounced in blends containing Type-II co-agents compared to those with Type-I co-agents. Notably, the delta torque value of silicone elastomers also increased with the addition of accelerators. TAC and TAIC exhibited higher torque values than ZDA and ZDMA, attributed to the former's possession of an extra vinyl group [11]. Also, When the CRI values of each prepared compound were examined, it was seen that the cure reactions occurred faster with the use of co-agent compared to the reference compound which did not contain co-agents. Type I co-agents cause a faster curing reaction than Type 2 co-agents because Type I co-agents create radicals with lower molecular weight and higher reactivity [7]. In addition, ZDA, one of the Type I co-agents, has a higher CRI value than ZDMA because ZDMA forms a more stable 3° radical due to the methyl group in its structure [15]. Furthermore, the compound containing co-agents demonstrated the highest CRI value, while the blend without co-agents exhibited the lowest. Co-agents were identified to enhance the cure rate by mitigating reactions that could compete with cross-linking, such as transfer and rearrangement reactions, distinct from cross-linking reactions [12,13].

4.2 The Cure rate constant (k) and activation energy (Ea) according to the first-order kinetic model

The k values calculated with first-order curing kinetics using the data of the rheometer curves of the prepared silicone elastomer blends are given in **Table 3**.

Table 3. First-order cure rate constant (k) of silicone compounds.

<i>Blends Code</i>	Cure Rate Constant. k (min⁻¹)				
	<i>170 °C</i>	<i>175 °C</i>	<i>180 °C</i>	<i>185 °C</i>	<i>190 °C</i>
VMQ	2.14±0.11	3.10±0.19	4.89±0.21	6.25±0.45	8.31±0.39
VMQ-TAC	1.65±0.07	2.54±0.11	3.48±0.15	5.08±0.32	7.28±0.40
VMQ-TAIC	1.89±0.10	2.95±0.11	4.14±0.22	5.65±0.27	7.81±0.35
VMQ-ZDA	3.10±0.14	4.52±0.21	6.29±0.27	8.79±0.36	11.22±0.58
VMQ-ZDMA	1.41±0.06	2.17±0.08	3.07±0.12	4.39±0.25	6.01±0.27
PVMQ	1.35±0.06	1.94±0.09	2.60±0.09	3.45±0.19	6.91±0.32
PVMQ-TAC	1.37±0.07	2.11±0.10	2.89±0.12	4.61±0.24	6.78±0.35
PVMQ-TAIC	1.53±0.08	2.21±0.09	3.39±0.17	5.11±0.25	7.13±0.29
PVMQ-ZDA	2.11±0.11	3.38±0.15	4.99±0.26	7.46±0.24	9.5±0.48
PVMQ-ZDMA	1.10±0.04	1.73±0.07	2.60±0.14	3.82±0.22	5.27±0.34

As presented in **Table 3**, it is clear that the rate constant (k) values increase with increasing temperatures in all compounds. Especially for VMQ-based elastomers, k values increased in elastomers containing TAC, TAIC, and ZDA compared to VMQ samples without coagent. At the same time, it was determined that the elastomer containing ZDMA had a lower k value compared to the k value of the reference compound without co-agent at all temperatures.

This observed decrease in k values for ZDMA can be attributed to the presence of a methyl group in its structure, which leads to steric hindrance as well as the formation of a more stable and less reactive tertiary radical. The highest k values in all compounds in the VMQ series were observed in ZDA, which is the Type I co-agent.

When elastomers prepared with PVMQ are examined, with the addition of the k -rate constant value TAC, TAIC, and ZDA, they have a higher reaction rate constant compared to the reference compound which has without co-agent. However, it is seen that the reaction rate decreases in the compound containing the Type I co-agent ZDMA. This trend can be attributed to the fact that ZDMA has a lower k value and forms a more stable 3° radical. However, it is interesting to observe that the k constant of samples prepared with VMQ is larger than those prepared with PVMQ. This difference can be attributed to the steric hindrance introduced by the phenyl group in the PVMQ structure.

Activation energies (E_a) of the elastomers were found by using the Arrhenius equation from the slope of the lines obtained by drawing $\ln k-1/T$ graphs from the k values found in the $\ln \alpha$ - time graphs of the elastomer compounds. At high temperatures, reactants can become thermally unstable. This means that additional reactions such as dissociation or recombination of chemical species may occur. This may cause the reaction rate to be different than expected. The $\ln k$ vs. $1/T$ graphs drawn using the k values calculated with the first-order curing kinetics of Type I and Type II co-agent-containing elastomers of VMQ, and PVMQ elastomers are given in **Fig. 2** and **Fig. 3**, respectively.

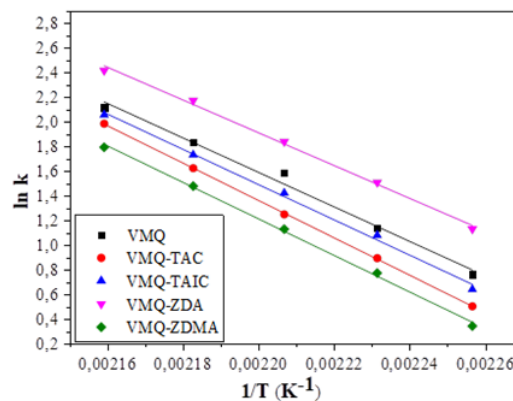


Figure 2. $\ln k$ versus ($1/T$) of VMQ silicone blends from Arrhenius equation at 170 °C, 175 °C, 180 °C, 185 °C and 190 °C.

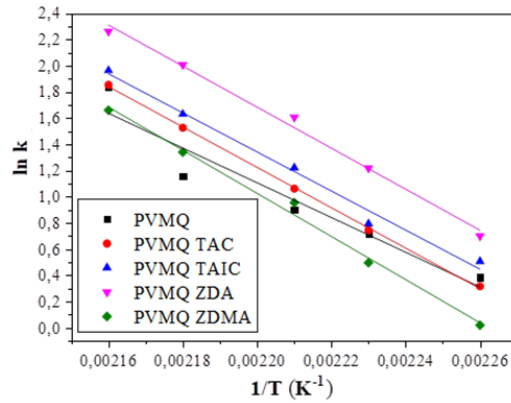


Figure 3. $\ln k$ versus $(1/T)$ of PVMQ silicone blends. from Arrhenius equation at 170 °C, 175 °C, 180 °C, 185 °C, and 190 °C.

As shown in **Table 4** activation energy does not change significantly with co-agent addition. The main reason for this is that in first-order curing kinetics, not the entire curing curve is evaluated, but the area where the cure rate (α) of 0.25-0.45 occurs. However, the activation energies of PVMQ samples are higher than VMQ samples.

Table 4. The activation energy (E_a) of silicone blends for the first order.

Blends Code	VMQ	VMQ-TAC	VMQ-TAIC	VMQ-ZDA	VMQ-ZDMA	PVMQ	PVMQ-TAC	PVMQ-TAIC	PVMQ-ZDA	PVMQ-ZDMA
E_a (kJ/mol)	116±8	126±3	119±5	111±6	123±4	129±3	136±2	134±9	130±8	135±8

4.3 The cure rate constant (k) and activation energy (E_a) according to n^{th} order kinetic model

After completing the first-order vulcanization kinetic analysis, a subsequent examination of all curing curves was conducted using the n^{th} -order kinetic model. This model, based on the methodology proposed by Isayev and Deng [14], involves a comprehensive analysis of the entire vulcanization curve from minimum torque (M_L) to maximum torque (M_H). The process includes the acquisition of α -time curves, representing the degree of cross-linking, and the application of Equation 5. Graphical interpretation using specialized software allows for the determination of the 'k' rate constant and 'n' reaction order values. The obtained 'k' values at different temperatures are then utilized in the Arrhenius equation to calculate the activation energy (E_a). This holistic approach provides valuable insights into the kinetics of the vulcanization reaction, offering information about the rate constant and reaction order dynamics across a range of temperatures.

According to **Equation 5**, the reaction rate constants of each blend at different temperatures "k" and the reaction rate degree "n" were determined by modeling using the Microcal Origin 7.5 software, the constants of the Deng–Isayev model were determined. **Fig. 4-a** and **4-b** present sample α -time curves for silicone elastomer compounds, with fitted curves obtained by solving these curves according to n^{th} -order cure kinetics (depicted in red). The curves in **Fig. 4-a** correspond to VMQ blends, while those in **Fig. 4-b** represent PVMQ compound. The reaction rate constants "k" and the reaction rate "n" of the silicone compound are given in **Table 5**. As can be seen in **Table 5**, the k values of all silicon blends increased with the increase in temperature. The reason for this increase is the molecular mobility that increases with temperature. Radicals with lower stability play a crucial role in enhancing the cure rate, as they exhibit a higher propensity for reaction. The diminished rate constant values observed in Type II accelerators compared to their Type I counterparts can be attributed to the radical stability inherent in the phenyl ring within the structure of Type II co-agents. This phenomenon has been previously discussed in the literature. Additionally, the participation of TAC and TAIC in reactions situated outside the cross-linking process contributes to the delayed formation of effective cross-linking, thereby lowering the rate constant of Type II accelerators [15].

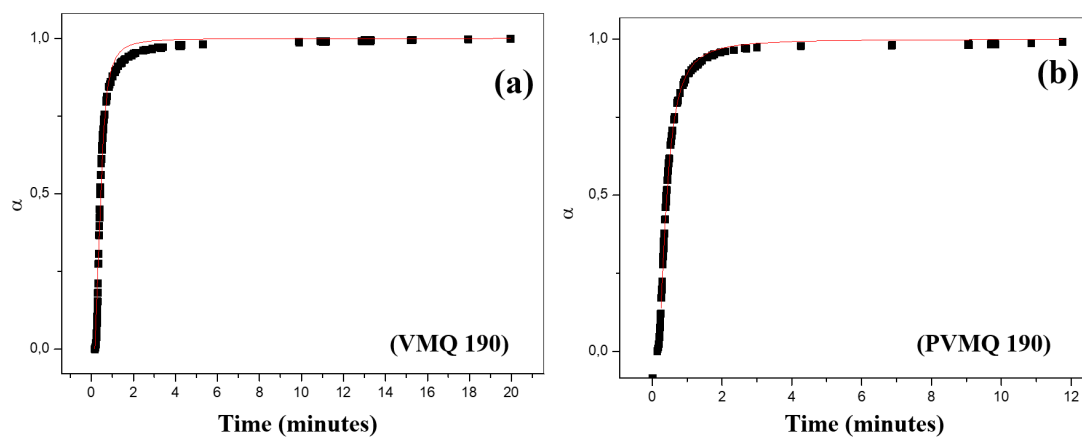


Figure 4. α -time curves of silicone elastomer blends and the curve fitted curve.

Notably, the structures of Type I accelerators, featuring acrylate and methacrylate, generate more reactive radicals, resulting in higher rate constant values when compared to their Type II counterparts. Further elucidating this trend, ZDMA exhibits lower rate constant values than ZDA, a phenomenon attributed to the formation of a more stable 3° radical due to the methyl group in its structure. As previously mentioned, the steric hindrance caused by this methyl group accounts for the observed disparity in rate constants.

Table 5. The cure rate constant (k) of silicone blends for n^{th} order.

Blends Code	Cure Rate Constant. k (min ⁻¹)					Reaction order. n				
	170 °C	175 °C	180 °C	185 °C	190 °C	170°C	175°C	180 °C	185°C	190°C
VMQ	2.8±0.2	3.6±0.2	4.9±0.3	6.7±0.7	9.0±0.6	0.8±0.0	0.8±0.0	0.8±0.0	0.8±0.1	0.8±0.1
VMQ-TAC	2.1±0.1	3.6±0.1	5.5±0.3	9.2±0.7	17.8±0.9	1.5±0.1	1.4±0.1	1.30±0.1	1.3±0.1	1.4±0.1
VMQ-TAIC	2.6±0.1	4.5±0.2	4.8±0.2	11.6±1.0	18.1±1.0	1.3±0.1	1.3±0.0	1.08±0.0	1.3±0.1	1.3±0.1
VMQ-ZDA	5.9±0.4	9.7±0.9	12.6±0.8	23.0±0.4	38.1±0.7	1.3±0.1	1.3±0.1	1.20±0.1	1.3±0.1	1.4±0.1
VMQ-ZDMA	2.2±0.1	3.5±0.2	6.1±0.5	9.0±0.9	15.6±0.4	1.3±0.1	1.2±0.1	1.4±0.1	1.3±0.1	1.3±0.1
PVMQ	1.9±0.1	2.2±0.2	2.6±0.1	3.2±0.2	9.1±0.16	0.6±0.1	0.5±0.1	0.6±0.0	0.6±0.0	0.8±0.1
PVMQ-TAC	1.9±0.1	3.2±0.2	4.9±0.3	8.3±0.8	13.4±0.5	1.3±0.1	1.2±0.1	1.3±0.1	1.2±0.1	1.3±0.1
PVMQ-TAIC	1.9±0.1	3.3±0.2	5.7±0.4	8.4±0.6	13.1±0.2	1.1±0.1	1.2±0.1	1.1±0.1	1.2±0.1	1.2±0.1
PVMQ-ZDA	2.9±0.3	5.2±0.4	8.2±0.6	10.9±0.6	17.5±0.5	1.0±0.4	1.1±0.1	1.1±0.1	1.0±0.1	1.2±0.0
PVMQ-ZDMA	1.6±0.1	2.7±0.1	4.5±0.2	7.3±0.8	10.3±0.4	1.3±0.1	1.1±0.1	1.3±0.1	1.2±0.1	1.1±0.1

The degree of reaction is associated with molecularity in simple chemical reactions [7]. In simpler terms, the degree of reaction is linked to the number of molecules that must collide at the appropriate geometry and energy for the chemical reaction to occur. As depicted in **Table 5**, the reaction degree of silicone elastomer without an accelerator is approximately 0.8. However, with the use of an accelerator, it is evident from the table that the 'n' value of the blends increases to an average of 1.2. This outcome signifies that accelerators are employed to enhance molecularity by altering the mechanism of the cross-linking reaction. The n^{th} cure rate constant and activation energy of silicone elastomers are further detailed in **Table 6**.

The k rate constant values of VMQ polymer show that the increase in k constant with temperature for TAC (from 2.1 min⁻¹ to 17.8 min⁻¹) and TAIC (from 2.6 min⁻¹ to 18.1 min⁻¹) is comparable. However, the results obtained for ZDA and ZDMA were found to be different. ZDA showed an increase in rate constant k from 5.9 min⁻¹ to 38.1 min⁻¹, but ZDMA showed an increase from 2.2 min⁻¹ to 15.6 min⁻¹. As mentioned before, steric hindrance of ZDMA is assumed to be responsible for this difference. Nevertheless, the k rate constant values do not vary much with the accelerator when the PVMQ polymer.

Table 6. The activation energy (Ea) of silicone blends for n^{th} order.

Blends Code	VMQ	VMQ-TAC	VMQ-TAIC	VMQ-ZDA	VMQ-ZDMA	PVMQ	PVMQ-TAC	PVMQ-TAIC	PVMQ-ZDA	PVMQ-ZDMA
Ea (kJ/mol)	217±8	281±6	308±6	308±9	255±8	171±8	254±4	258±6	233±7	225±8

It can be seen in **Table 5**; that the reaction rate increases with the increase of temperature for all samples. Reaction order and rate constants values are higher than first order because n^{th} order calculation comprises all curves. The highest k-constant values were observed in samples containing ZDA. In comparison, the lowest k values were observed in samples containing ZDMA. As shown in Table 6, the calculated activation energies from the n^{th} order are also higher than the first order. Activation energy values obtained from compounds containing Type II co-agents were found to be higher than the activation energy values obtained from compounds containing Type I co-agents.

It has been found that the reaction rate constants in the n^{th} -order cure kinetics of most prepared elastomers are higher than those in the first-order cure kinetics. This indicates that co-agents increase the cure rate by mitigating transfer and rearrangement reactions that compete with cross-linking reactions. The PVMQ, and VMQ elastomers without co-agents, however, have lower rate constants because they do not exhibit this effect. For example, in Table 3, the reaction rate constants for VMQ and VMQ-ZDA elastomers at an optimal cure temperature of 180°C were found to be $4.9 \pm 0.3 \text{ min}^{-1}$ and $6.3 \pm 0.3 \text{ min}^{-1}$, respectively, in first-order cure kinetics calculations. Additionally, the reaction rate constants for PVMQ and PVMQ-ZDA were $2.6 \pm 0.1 \text{ min}^{-1}$ and $5.0 \pm 0.3 \text{ min}^{-1}$, respectively. In the n^{th} -order cure kinetics calculations given in Table 5, the reaction rate constants at 180°C for the VMQ and VMQ-ZDA compounds were $4.9 \pm 0.3 \text{ min}^{-1}$ for the VMQ compound without co-agents, showing no significant change, while the VMQ-ZDA compound had a rate constant of $12.6 \pm 0.8 \text{ min}^{-1}$, approximately two times higher. The reaction rate constant for PVMQ was $2.6 \pm 0.1 \text{ min}^{-1}$, and for PVMQ-ZDA it was found to be $8.2 \pm 0.6 \text{ min}^{-1}$, which is approximately 65% higher. The primary reason for this is that in the first-order cure kinetics, the cure state (α) values in the range of 0.25-0.40 are considered, whereas in the n^{th} -order cure kinetics, the entire cure curve is included in the calculation. As previously stated, in the first-order cure kinetics, the reaction order (n) was assumed to be 1. However, in the n^{th} -order cure kinetics, the reaction orders for VMQ and PVMQ without co-agents were found to be 0.80 ± 0.01 and 0.70 ± 0.01 , respectively. Additionally, the reaction order values for all compounds containing co-agents were found to be approximately 1.2 on average. This indicates the positive effect of co-agent usage on cross-linking reactions. The activation energy values in Table 6 are higher than those given in Table 4 because the E_a values in Table 6 are obtained by evaluating the entire cure curves. The E_a values of PVMQ and VMQ compounds containing co-agents were found to be approximately 40% higher than those of the compounds without co-agents. The Δ torque value, which is a measure of cross-link density, increased by approximately 61% with the use of co-agents.

Comparative activation energy bar graphs of silicone elastomer blends found using 1st and nth-order curing kinetic models are given in **Fig. 5**.

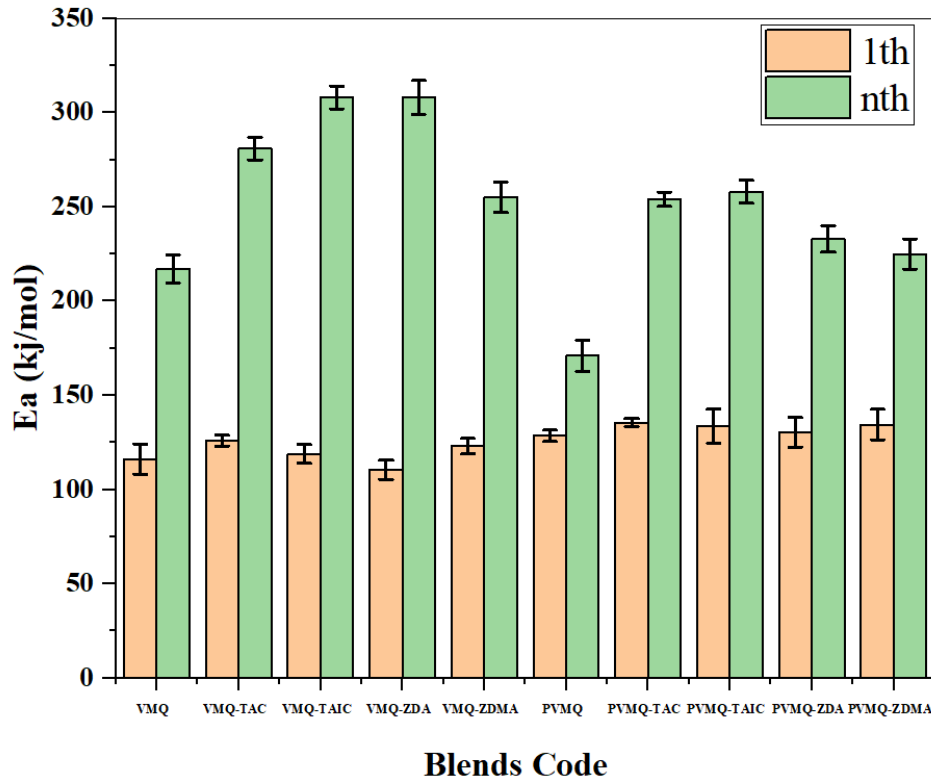


Figure 5. Comparative activation energy bar graphs of silicone elastomer blends.

As can be seen in **Fig. 5**, the activation energies found at n order were higher than the activation energies found at 1 order. This is because the 0.25/0.40 range of the α (degree of crosslinking value) is used in calculations from 1st, while the entire cure curve is used in nth cure kinetics.

5. Conclusion

It has been observed that the use of co-agents increased the curing reactions and efficiency of the state of cure value in silicone elastomers cured with peroxide. Because co-agents prevent reactions other than cross-linking, such as transfer and rearrangement, that compete with the cross-linking reaction. It was observed that the activation energy values obtained with the nth nth kinetic model were higher than the values obtained with the first-order kinetic model, since they were the values obtained by using the cure reaction or the entire cure curve. For this reason, it is necessary to use the nth kinetic model to find the activation energy. When the 1st degree activation energies are examined, it is seen that the activation energies obtained for PVMQ are higher than

the activation energies obtained for VMQ. This is thought to be due to the steric hindrance of the phenyl group in the structure of the PVMQ elastomer. When the n^{th} activation energies are examined, it is seen that the activation energies obtained for VMQ are higher than the activation energies obtained for PVMQ. This is because VMQ has a higher degree of reactivity, so more molecules must cross the energy barrier for the cross-linking reaction. While the use of co-agents has been shown to affect the curing behavior and rheology of silicone elastomers, it is clear that the elastomer components and type of manufacturing process will affect the performance of the final product.

References

- [1] Jerschow, P., & Wacker-Chemie GmbH., *Silicone Elastomers Report 137*. In *Rapra Review Reports*, 12, (5), 2001.
- [2] S.K. Henning & R. Costin, *Fundamentals of curing elastomers with peroxides and coagents*, *Rubber World* 233(5):28-35, 2006.
- [3] Wang H, Ding Y & Zhao S., *Effects of Co-Agents on the Properties of Peroxide-Cured Ethylene-Propylene Diene Rubber (EPDM)*, *Journal Of Macromolecular Science, Part B: Physics*, 55(5), 433–444, 2016.
- [4] Palys, L. H. & Callais, P. An A., *Understanding Organic Peroxides to Obtain Optimal Crosslinking Performance*. *Rubber World*, 229:11, 35, 2003.
- [5] Kaymazlar E., *Effect of Accelerator Type and Ratio on The Relaxation Behaviors of Silicone Elastomers*, Master's Thesis, Ondokuz Mayıs University Graduate School of Sciences Department of Chemistry, Samsun, Turkey, 2018.
- [6] Kruželák J, Kvasničáková A, Hložeková K & Hudec, *Influence of dicumyl peroxide and Type I and II coagents on cross-linking and physical–Mechanical properties of rubber compounds based on NBR*, *Plastics, Rubber and Composites*, 49(8):1-14, 2020.
- [7] V. Bheemreddy, Z. Huo, K. Chandrashekhara & R. A. Brack, *Modeling and simulation of cure kinetics and flow in cavity-molded composites*, *Journal of The American Helicopter Society* 61, 022004, 2016.
- [8] Atkins, P.; de Paula, J. *Physical Chemistry. Part 2, 22 The rates of chemical reactions*, Oxford University Press. page 791, 2014.
- [9] I Surya, L Sukeksi & N Hayeemasae, *Studies on cure index, swelling behaviour, tensile and thermooxidative properties of natural rubber compounds in the presence of alkanolamide*, *IOP Conf. Series: Materials Science and Engineering* 309 012060, 2018.
- [10] Ding, R., Leonov, A. I. ve Coran, A. Y., *A study of the vulcanization kinetics of an accelerated-sulfur SBR compound*, *Rubber Chemistry and Technology*, 69: 1, 81–91, 1996.
- [11] Yang, Sen lin, Zhi Hua Wu, Wei Yang, & Ming Bo Yang, *Thermal and Mechanical Properties of Chemical Crosslinked Polylactide (PLA)*, *Polymer Testing* 27(8):957–63, 2008.
- [12] García-Quesada, J. C. & Gilbert, M., *Peroxide crosslinking of unplasticized poly(vinyl chloride)*, *Journal of Applied Polymer Science*, 77: 12, 2657–2666, 2000.
- [13] Búcsi, A. ve Szöcs, F., *Kinetics of radical generation in PVC with dibenzoyl peroxide utilizing High-Pressure Technique*, *Macromolecular Chemistry, and Physics*, 201: 4, 435–438, 2020.

[14] Isayev, A.I., Deng, J.S., *Non-isothermal vulcanization of rubber compounds*, *Rubber Chem Technol*, 61, 340-361, 1998.

[15] Dikland, H. G., Ruardy, T., Vanderdoes, L. ve Bantjes, A., *New Coagents in Peroxide Vulcanization of Edpm*, *Rubber Chemistry and Technology*, 66: 5, 693–711, 1993.

[16] I. Surya, H. Ismail, A.R. Azura, *Alkanolamide as an accelerator, filler-dispersant and a plasticizer in silica-filled natural rubber compounds*, *Polym. Test.*, 32, 1313-1321, 2013.



On New Spinor Sequences of Jacobsthal and Jacobsthal-Lucas Quaternions

Tülay ERİŞİR^{1,*}, Mehmet Ali GÜNGÖR²

¹*Erzincan Binali Yıldırım University, Department of Mathematics, 24002, Erzincan, Türkiye*
tulay.erisir@erzincan.edu.tr, ORCID: 0000-0001-6444-1460

²*Sakarya University, Department of Mathematics, 54187, Sakarya, Türkiye*
agungor@sakarya.edu.tr, ORCID: 0000-0003-1863-3183

Received: 04.04.2024

Accepted: 14.06.2024

Published: 28.06.2024

Abstract

In this study, two new spinor sequences using spinor representations of Jacobsthal and Jacobsthal-Lucas quaternions are defined. Moreover, some formulas such that Binet, Cassini, summation formulas and generating functions of these spinor sequences, which are called as Jacobsthal and Jacobsthal-Lucas spinor sequences, are expressed. Then, some relationships between Jacobsthal and Jacobsthal-Lucas spinors are obtained. Therefore, an easier and more interesting representation of Jacobsthal and Jacobsthal-Lucas quaternions, which are generalization of Jacobsthal and Jacobsthal-Lucas number sequences, are obtained. We believe that these new spinor sequences will be useful and advantageable in many branches of science, such as geometry, algebra and physics.

Keywords: Jacobsthal numbers; Jacobsthal-Lucas numbers; Quaternions; Spinors.

Jacobsthal ve Jacobsthal-Lucas Kuaterniyonlarının Yeni Spinor Dizileri Üzerine

Öz

Bu çalışmada Jacobsthal ve Jacobsthal-Lucas kuaterniyonlarının spinör gösterimleri kullanılarak iki yeni spinor dizisi tanımlanmıştır. Ayrıca, Jacobsthal ve Jacobsthal-Lucas spinor dizileri olarak adlandırılan bu spinor dizilerinin Binet, Cassini, toplam formülleri ve üreteç fonksiyonları gibi bazı formüller ifade edilmiştir. Daha sonra Jacobsthal ve Jacobsthal-Lucas



spinorları arasındaki bazı ilişkiler elde edilmiştir. Böylece Jacobsthal ve Jacobsthal-Lucas sayı dizilerinin genellemesi olan Jacobsthal ve Jacobsthal-Lucas kuaterniyonlarının daha kolay ve ilginç bir temsili elde edilmiş olur. Bu yeni spinor dizilerinin geometri, cebir ve fizik gibi birçok bilim dalında faydalı ve avantajlı olacağına inanmaktayız.

Anahtar Kelimeler: Jacobsthal sayıları; Jacobsthal-Lucas sayıları; Kuaterniyonlar; Spinorlar.

1. Introduction

The first known number sequence is the Fibonacci number sequence expressed by Fibonacci (1170-1250), which is frequently encountered in nature [1-3]. The Lucas number sequence is another example of a number sequence. In addition, there are many number sequences in the literature. Moreover, considering different characteristic equations and initial values, different number sequences can be obtained in [4-6]. Other studies of this subject are [7-11] Horadam discussed Pell numbers and their properties [5]. On the other hand, Horadam gave Jacobsthal and Jacobsthal-Lucas number sequences [4]. Daşdemir studied on the Jacobsthal numbers in [12]. In [13] the Jacobsthal quaternions were expressed. Then, a new approach to Jacobsthal quaternions were obtained in [14]. Halıcı expressed bicomplex Jacobsthal-Lucas numbers [15]. Moreover, in the other study [16], the new recurrences were obtained. Arslan obtained the complex gaussian Jacobsthal quaternions [17]. Özkan end Uysal expressed the higher order Jacobsthal quaternions [18]. Moreover, the $J(r, n)$ -Jacobsthal quaternions were obtained in [19]. Other studies can be given in [20,21].

Spinor whose transformation is associated to spins in physics can be defined as vectors of a geometric space basically. Geometrically, Cartan introduced spinors [22]. Cartan's study [22] is an admirable study in spinor geometry because in that study, the spinor representations of some geometric expressions were expressed in an easy and understandable way. Another inspiring study on the spinors in geometry was done by Vivarelli [23]. In [23], the relationship between quaternions and spinor representations of rotations with three dimensional were obtained. In the study [24], the spinor representations of the Frenet frame and curvatures of any curve in E^3 were given. Darboux spinor equations in E^3 were obtained [25]. Moreover, in [26], the spinor Bishop frame in E^3 was expressed. The spinor equations for some special curves such as Bertrand, involute-evolute, successor, Mannheim curves, Sabban frames, and Lie groups were obtained in [27-32]. Then, for any Minkowski space, the hyperbolic spinor equations were given [33-36]. In addition to that, Fibonacci and Lucas spinors were expressed in [37].

2. Materials and Methods

Now, the spinors, real quaternions, relationships between them spinors, and Jacobsthal, Jacobsthal-Lucas quaternions are given.

Suppose that any isotropic vector is $v = (v_1, v_2, v_3) \in C^3$ where $v_1^2 + v_2^2 + v_3^2 = 0$ and the complex vector 3-space is C^3 . We can express the set of isotropic vectors in C^3 with the aid of a two-dimensional surface in C^2 . Suppose that this surface has coordinates ϖ_1 and ϖ_2 . So, we can write $v_1 = \varpi_1^2 - \varpi_2^2$, $v_2 = \mathbf{i}(\varpi_1^2 + \varpi_2^2)$, $v_3 = -2\varpi_1\varpi_2$ and $\varpi_1 = \pm\sqrt{\frac{v_1 - \mathbf{i}v_2}{2}}$, $\varpi_2 = \pm\sqrt{\frac{-v_1 - \mathbf{i}v_2}{2}}$. This two-dimensional complex vector is called as spinor

$$\varpi = (\varpi_1, \varpi_2) = \begin{bmatrix} \varpi_1 \\ \varpi_2 \end{bmatrix}$$

[22].

Suppose that any real quaternion is $r = r_0 + \mathbf{i}r_1 + \mathbf{j}r_2 + \mathbf{k}r_3$ where $r_0, r_1, r_2, r_3 \in R$. $\{\mathbf{1}, \mathbf{i}, \mathbf{j}, \mathbf{k}\}$ is called the quaternion basis such that

$$\mathbf{i}^2 = \mathbf{j}^2 = \mathbf{k}^2 = -1, \quad \mathbf{ij} = -\mathbf{j\i} = \mathbf{k}, \quad \mathbf{jk} = -\mathbf{kj} = \mathbf{i}, \quad \mathbf{ki} = -\mathbf{ik} = \mathbf{j}$$

[38]. We can write $r = S_r + \mathbf{V}_r$ where $r_0 = S_r$ and $\mathbf{V}_r = \mathbf{i}r_1 + \mathbf{j}r_2 + \mathbf{k}r_3$ is called scalar and vector parts of r , respectively [38]. Assume that two any real quaternions $p = S_p + \mathbf{V}_p$, $r = S_r + \mathbf{V}_r$. So, the quaternion product is also

$$r \times p = S_r S_p - \langle \mathbf{V}_r, \mathbf{V}_p \rangle + S_r \mathbf{V}_p + S_p \mathbf{V}_r + \mathbf{V}_r \wedge \mathbf{V}_p$$

[38]. We know that this operation is non-commutative. In addition to that, the quaternion conjugate and the norm of r are expressed as $r^* = S_r - \mathbf{V}_r$ and $N(r) = \sqrt{r_1^2 + r_2^2 + r_3^2 + r_4^2}$. The norm of r be $N(r) = 1$ then, r is called as unit quaternion [38].

Vivarelli expressed a relation between spinors and quaternions with following transformation

$$f: H \rightarrow S$$

$$r \rightarrow f(r_0 + \mathbf{i}r_1 + \mathbf{j}r_2 + \mathbf{k}r_3) \cong \begin{bmatrix} r_3 + \mathbf{i}r_0 \\ r_1 + \mathbf{i}r_2 \end{bmatrix} \equiv \varpi \quad (1)$$

where $r = r_0 + \mathbf{i}r_1 + \mathbf{j}r_2 + \mathbf{k}r_3$ is any real quaternion [18]. The spinor representation of $r \times p$ such that

$$r \times p \rightarrow -\mathbf{i}\hat{\varpi}\rho \quad (2)$$

where the spinor ρ corresponds to the p considering f in the equation (1) and the complex, unitary, square matrix $\hat{\varpi}$ can be written as

$$\hat{\varpi} = \begin{bmatrix} r_3 + \mathbf{i}r_0 & r_1 - \mathbf{i}r_2 \\ r_1 + \mathbf{i}r_2 & -r_3 + \mathbf{i}r_0 \end{bmatrix} \quad (3)$$

[23]. In addition, the spinor matrix $\varpi_L = -\mathbf{i}\hat{\varpi}$, namely

$$\varpi_L = \begin{bmatrix} r_0 - \mathbf{i}r_3 & -r_2 - \mathbf{i}r_1 \\ r_2 - \mathbf{i}r_1 & r_0 + \mathbf{i}r_3 \end{bmatrix} \quad (4)$$

was called the fundamental spinor matrix or the left Hamilton spinor matrix of r [23, 39].

Now, some equalities about the Jacobsthal and Jacobsthal-Lucas quaternions given in [13, 14] can be expressed. For $n \geq 2$ the n th Jacobsthal and Jacobsthal-Lucas quaternions are defined that

$$JQ_n = J_n + \mathbf{i}J_{n+1} + \mathbf{j}J_{n+2} + \mathbf{k}J_{n+3}$$

and

$$JLQ_n = JL_n + \mathbf{i}JL_{n+1} + \mathbf{j}JL_{n+2} + \mathbf{k}JL_{n+3}$$

where the n th Jacobsthal number and Jacobsthal-Lucas number $J_n = J_{n-1} + 2J_{n-2}$ ($J_0 = 0, J_1 = 1$) and $JL_n = JL_{n-1} + 2JL_{n-2}$ ($JL_0 = 2, JL_1 = 1$) [13, 14]. Therefore, the recurrence relations of the Jacobsthal and Jacobsthal-Lucas quaternions for $n \geq 2$ are

$$JQ_n = JQ_{n-1} + 2JQ_{n-2}$$

with initial conditions $JQ_0 = \mathbf{i} + \mathbf{j} + 3\mathbf{k}$, $JQ_1 = 1 + \mathbf{i} + 3\mathbf{j} + 5\mathbf{k}$ and

$$JLQ_n = JLQ_{n-1} + 2JLQ_{n-2}$$

with initial conditions $JLQ_0 = 2 + \mathbf{i} + 5\mathbf{j} + 7\mathbf{k}$, $JLQ_1 = 1 + 5\mathbf{i} + 7\mathbf{j} + 17\mathbf{k}$ [13, 14].

Now, we write some relationships between the Jacobsthal and Jacobsthal-Lucas quaternions with the aid of [13, 14]. Therefore, the Binet formulas for the Jacobsthal and Jacobsthal-Lucas quaternions are given that

$$JQ_n = \frac{1}{\alpha - \beta} (\alpha^n \underline{\alpha} - \beta^n \underline{\beta})$$

and

$$JLQ_n = \alpha^n \underline{\alpha} + \beta^n \underline{\beta}$$

where the quaternions $\underline{\alpha}$ and $\underline{\beta}$ are $\underline{\alpha} = 1 + \alpha\mathbf{i} + \alpha^2\mathbf{j} + \alpha^3\mathbf{k} = 1 + 2\mathbf{i} + 4\mathbf{j} + 8\mathbf{k}$ and $\underline{\beta} = 1 + \beta\mathbf{i} + \beta^2\mathbf{j} + \beta^3\mathbf{k} = 1 - \mathbf{i} + \mathbf{j} - \mathbf{k}$, $\alpha = 2$, $\beta = -1$ are roots of the characteristic equation $x^2 - x - 2 = 0$. On the other hand, we give Cassini formulas for the Jacobsthal and Jacobsthal-Lucas quaternions can be given that

$$JQ_{n-1}JQ_{n+1} - (JQ_n)^2 = (-1)^n 2^{n-1} (7 + 5\mathbf{i} + 7\mathbf{j} + 5\mathbf{k})$$

and

$$JLQ_{n-1}JLQ_{n+1} - (JLQ_n)^2 = (-2)^{n-1} 3^2 (7 + 5\mathbf{i} + 7\mathbf{j} + 5\mathbf{k}),$$

respectively [13,14].

3. Results and Discussion

In this section, we define relationships between Jacobsthal, Jacobsthal-Lucas quaternions and spinors and, express the spinors corresponding to Jacobsthal and Jacobsthal-Lucas quaternions. Therefore, we call as Jacobsthal spinor and Jacobsthal-Lucas spinor associated with Jacobsthal and Jacobsthal-Lucas quaternions. Then, we give some relationships between Jacobsthal spinor and Jacobsthal-Lucas spinor. We obtain some formulas such that Binet, Cassini, summation formulas and generating functions for these spinors and some theorems.

Definition 1. Let $JQ_n = J_n + \mathbf{i}J_{n+1} + \mathbf{j}J_{n+2} + \mathbf{k}J_{n+3}$ be n th Jacobsthal quaternion where J_n is n th Jacobsthal number and the set of Jacobsthal quaternions be H_J . Then, the following linear transformation

$$f_J : H_J \rightarrow S$$

$$JQ_n \rightarrow f_J(JQ_n) \cong SJ_n = \begin{bmatrix} J_{n+3} + \mathbf{i}J_n \\ J_{n+1} + \mathbf{i}J_{n+2} \end{bmatrix} \quad (5)$$

can be obtain where $\mathbf{i}, \mathbf{j}, \mathbf{k}$ coincide with basis vectors in \sim^3 and $\mathbf{i}^2 = -1$. So, a new spinor sequence corresponding Jacobsthal quaternions is called as "Jacobsthal Spinor Sequence" such as

$$\{SJ_n\}_{n \in \mathbb{N}}^\infty = \left\{ \begin{bmatrix} 3 \\ 1 + \mathbf{i} \end{bmatrix}, \begin{bmatrix} 5 + \mathbf{i} \\ 1 + 3\mathbf{i} \end{bmatrix}, \begin{bmatrix} 11 + \mathbf{i} \\ 3 + 5\mathbf{i} \end{bmatrix}, \begin{bmatrix} 21 + 3\mathbf{i} \\ 5 + 11\mathbf{i} \end{bmatrix}, \dots \right\}$$

where $SJ_n = \begin{bmatrix} J_{n+3} + \mathbf{i}J_n \\ J_{n+1} + \mathbf{i}J_{n+2} \end{bmatrix}$ is n th Jacobsthal spinor and J_n is n th Jacobsthal number.

Similarly, we can give the following definition of Jacobsthal-Lucas spinor sequence.

Definition 2. Assume that $JLQ_n = JL_n + \mathbf{i}JL_{n+1} + \mathbf{j}JL_{n+2} + \mathbf{k}JL_{n+3}$ is n th Jacobsthal-Lucas quaternion where JL_n is n th Jacobsthal-Lucas number. The n th Jacobsthal-Lucas quaternion

JLQ_n matches the spinor $JLQ_n \rightarrow SJL_n = \begin{bmatrix} JL_{n+3} + \mathbf{i}JL_n \\ JL_{n+1} + \mathbf{i}JL_{n+2} \end{bmatrix}$. Then, a new spinor sequence

corresponding Jacobsthal-Lucas quaternions is defined as "Jacobsthal-Lucas Spinor Sequence"

$$\{SJL_n\}_{n \in \mathbb{N}}^\infty = \left\{ \begin{bmatrix} 7 + 2\mathbf{i} \\ 1 + 5\mathbf{i} \end{bmatrix}, \begin{bmatrix} 17 + \mathbf{i} \\ 5 + 7\mathbf{i} \end{bmatrix}, \begin{bmatrix} 31 + 5\mathbf{i} \\ 7 + 17\mathbf{i} \end{bmatrix}, \begin{bmatrix} 65 + 7\mathbf{i} \\ 17 + 31\mathbf{i} \end{bmatrix}, \dots \right\} \text{ where } SJL_n = \begin{bmatrix} JL_{n+3} + \mathbf{i}JL_n \\ JL_{n+1} + \mathbf{i}JL_{n+2} \end{bmatrix} \text{ is } n\text{th}$$

Jacobsthal-Lucas spinor and JL_n is n th Jacobsthal-Lucas number.

Definition 3. The conjugate of Jacobsthal quaternion JQ_n is JQ_n^* , and Jacobsthal spinor corresponding to this conjugate is defined as

$$SJ_n^* = \begin{bmatrix} -J_{n+3} + \mathbf{i}J_n \\ -J_{n+1} - \mathbf{i}J_{n+2} \end{bmatrix}.$$

Similarly, the Jacobsthal-Lucas spinor corresponding to the conjugate of Jacobsthal-Lucas quaternion JLQ_n is defined as

$$SJL_n^* = \begin{bmatrix} -JL_{n+3} + \mathbf{i}JL_n \\ -JL_{n+1} - \mathbf{i}JL_{n+2} \end{bmatrix}.$$

Definition 4. The Jacobsthal spinor representation of the norm of Jacobsthal quaternion JQ_n is $\overline{SJ_n}^t SJ_n$. Similarly, the Jacobsthal-Lucas spinor representation of the norm of Jacobsthal-Lucas quaternion JLQ_n is $\overline{SJL_n}^t SJL_n$.

Now, the recurrence relations of Jacobsthal and Jacobsthal-Lucas spinor sequences with the following equations should be stated.

Theorem 5. The recurrence relation of Jacobsthal spinors is

$$SJ_{n+2} = SJ_{n+1} + 2SJ_n$$

where n th, $(n+1)$ th and $(n+2)$ th Jacobsthal spinors are SJ_n , SJ_{n+1} , and SJ_{n+2} , respectively. The recurrence relation for Jacobsthal-Lucas spinor is

$$SJL_{n+2} = SJL_{n+1} + 2SJL_n$$

where n th, $(n+1)$ th and $(n+2)$ th Jacobsthal-Lucas spinors are SJL_n , SJL_{n+1} , and SJL_{n+2} , respectively.

Proof: We show the recurrence relation for Jacobsthal spinors in first. Therefore, if we calculate $SJ_{n+1} + 2SJ_n$, then we obtain

$$SJ_{n+1} + 2SJ_n = \begin{bmatrix} J_{n+4} + \mathbf{i}J_{n+1} \\ J_{n+2} + \mathbf{i}J_{n+3} \end{bmatrix} + 2 \begin{bmatrix} J_{n+3} + \mathbf{i}J_n \\ J_{n+1} + \mathbf{i}J_{n+2} \end{bmatrix} = \begin{bmatrix} J_{n+4} + 2J_{n+3} + \mathbf{i}(J_{n+1} + 2J_n) \\ J_{n+2} + 2J_{n+1} + \mathbf{i}(J_{n+3} + 2J_{n+2}) \end{bmatrix}.$$

Since the recurrence relation for Jacobsthal number sequence is $SJ_{n+2} = SJ_{n+1} + 2SJ_n$ in [4], we have

$$SJ_{n+1} + 2SJ_n = \begin{bmatrix} J_{n+5} + \mathbf{i}J_{n+2} \\ J_{n+3} + \mathbf{i}J_{n+4} \end{bmatrix} = SJ_{n+2}.$$

Similarly, we can easily obtain for Jacobsthal-Lucas spinor sequence such that

$$SJL_{n+1} + 2SJL_n = \begin{bmatrix} JL_{n+4} + 2JL_{n+3} + \mathbf{i}(JL_{n+1} + 2JL_n) \\ JL_{n+2} + 2JL_{n+1} + \mathbf{i}(JL_{n+3} + 2JL_{n+2}) \end{bmatrix} = \begin{bmatrix} JL_{n+5} + \mathbf{i}JL_{n+2} \\ JL_{n+3} + \mathbf{i}JL_{n+4} \end{bmatrix} = SJL_{n+2}.$$

where we use the recurrence relation of the Jacobsthal Lucas number sequence $SJL_{n+2} = SJL_{n+1} + 2SJL_n$ in [4].

Now, we can give the some equations about Jacobsthal and Jacobsthal-Lucas spinors.

Theorem 6. Suppose that n th, $(n+1)$ th, $(n+r)$ th, and $(n-r)$ th Jacobsthal spinors are SJ_n , SJ_{n+1} , SJ_{n+r} , and SJ_{n-r} , respectively. In this case, for $n \geq 1$, $r \geq 1$ there are the following relations;

$$\begin{aligned} i) \quad & SJ_{n+1} + SJ_n = 2^n S_\alpha, \\ ii) \quad & SJ_{n+1} - SJ_n = \frac{1}{3} \left[2^n S_\alpha + 2(-1)^n S_\beta \right], \\ iii) \quad & SJ_{n+r} + SJ_{n-r} = \frac{1}{3} \left[2^{n-r} (2^{2r} + 1) S_\alpha - 2(-1)^{n-r} S_\beta \right], \\ iv) \quad & SJ_{n+r} - SJ_{n-r} = \frac{1}{3} 2^{n-r} (2^{2r} - 1) S_\alpha \end{aligned}$$

where the spinors S_α and S_β are $S_\alpha = \begin{bmatrix} \alpha^3 + \mathbf{i} \\ \alpha + \mathbf{i}\alpha^2 \end{bmatrix} = \begin{bmatrix} 8 + \mathbf{i} \\ 2 + 4\mathbf{i} \end{bmatrix}$ and

$$S_\beta = \begin{bmatrix} \beta^3 + \mathbf{i} \\ \beta + \mathbf{i}\beta^2 \end{bmatrix} = \begin{bmatrix} -1 + \mathbf{i} \\ -1 + \mathbf{i} \end{bmatrix} = (-1 + \mathbf{i}) \begin{bmatrix} 1 \\ 1 \end{bmatrix}, \text{ respectively.}$$

Proof:

i) Assume that n th and $(n+1)$ th Jacobsthal spinors are SJ_n and SJ_{n+1} , respectively.

Then, we can write the equation

$$SJ_{n+1} + SJ_n = \begin{bmatrix} J_{n+4} + \mathbf{i}J_{n+1} \\ J_{n+2} + \mathbf{i}J_{n+3} \end{bmatrix} + \begin{bmatrix} J_{n+3} + \mathbf{i}J_n \\ J_{n+1} + \mathbf{i}J_{n+2} \end{bmatrix} = \begin{bmatrix} J_{n+4} + J_{n+3} + \mathbf{i}(J_{n+1} + J_n) \\ J_{n+2} + J_{n+1} + \mathbf{i}(J_{n+3} + J_{n+2}) \end{bmatrix}.$$

On the other hand, we know that $J_{n+1} + J_n = 2^n$ in [4]. Therefore, we obtain

$$SJ_{n+1} + SJ_n = \begin{bmatrix} 2^{n+3} + \mathbf{i}2^n \\ 2^{n+1} + \mathbf{i}2^{n+2} \end{bmatrix} = 2^n \begin{bmatrix} 8 + \mathbf{i} \\ 2 + 4\mathbf{i} \end{bmatrix} = 2^n S_\alpha$$

where $S_\alpha = \begin{bmatrix} \alpha^3 + \mathbf{i} \\ \alpha + \mathbf{i}\alpha^2 \end{bmatrix} = \begin{bmatrix} 8 + \mathbf{i} \\ 2 + 4\mathbf{i} \end{bmatrix}$.

ii) We suppose that n th and $(n+1)$ th Jacobsthal spinors are SJ_n and SJ_{n+1} , respectively. We can write

$$SJ_{n+1} - SJ_n = \begin{bmatrix} J_{n+4} + \mathbf{i}J_{n+1} \\ J_{n+2} + \mathbf{i}J_{n+3} \end{bmatrix} - \begin{bmatrix} J_{n+3} + \mathbf{i}J_n \\ J_{n+1} + \mathbf{i}J_{n+2} \end{bmatrix} = \begin{bmatrix} J_{n+4} - J_{n+3} + \mathbf{i}(J_{n+1} - J_n) \\ J_{n+2} - J_{n+1} + \mathbf{i}(J_{n+3} - J_{n+2}) \end{bmatrix}.$$

If we use the equation $J_{n+1} - J_n = \frac{1}{3}(2^n - 2(-1)^{n+1})$ for Jacobsthal numbers in [4] then, we get

$$\begin{aligned} SJ_{n+1} + SJ_n &= \begin{bmatrix} \frac{1}{3}(2^{n+3} - 2(-1)^{n+4}) + \mathbf{i}\frac{1}{3}(2^n - 2(-1)^{n+1}) \\ \frac{1}{3}(2^{n+1} - 2(-1)^{n+2}) + \mathbf{i}\frac{1}{3}(2^{n+2} - 2(-1)^{n+3}) \end{bmatrix} \\ &= \frac{1}{3} \left(2^n \begin{bmatrix} 8 + \mathbf{i} \\ 2 + 4\mathbf{i} \end{bmatrix} - 2(-1)^{n+1} \begin{bmatrix} -1 + \mathbf{i} \\ -1 + \mathbf{i} \end{bmatrix} \right) = \frac{1}{3} (2^n S_\alpha + 2(-1)^n S_\beta) \end{aligned}$$

where the spinors S_α and S_β are $S_\alpha = \begin{bmatrix} \alpha^3 + \mathbf{i} \\ \alpha + \mathbf{i}\alpha^2 \end{bmatrix} = \begin{bmatrix} 8 + \mathbf{i} \\ 2 + 4\mathbf{i} \end{bmatrix}$ and

$$S_\beta = \begin{bmatrix} \beta^3 + \mathbf{i} \\ \beta + \mathbf{i}\beta^2 \end{bmatrix} = \begin{bmatrix} -1 + \mathbf{i} \\ -1 + \mathbf{i} \end{bmatrix} = (-1 + \mathbf{i}) \begin{bmatrix} 1 \\ 1 \end{bmatrix}, \text{ respectively.}$$

iii) Let $(n+r)$ th and $(n-r)$ th Jacobsthal spinors be SJ_{n+r} and SJ_{n-r} , respectively.

Moreover, we know that there is the equation $J_{n+r} + J_{n-r} = \frac{1}{3}(2^{n-r}(2^{2r} + 1) - 2(-1)^{n-r})$ for Jacobsthal numbers in [4]. Therefore, we obtain that

$$\begin{aligned} SJ_{n+r} + SJ_{n-r} &= \begin{bmatrix} J_{n+r+3} + J_{n-r+3} + \mathbf{i}(J_{n+r} + J_{n-r}) \\ J_{n+r+1} + J_{n-r+1} + \mathbf{i}(J_{n+r+2} - J_{n-r+2}) \end{bmatrix} \\ &= \frac{1}{3} \left(2^{n-r} (2^{2r} + 1) \begin{bmatrix} 8 + \mathbf{i} \\ 2 + 4\mathbf{i} \end{bmatrix} - 2(-1)^{n-r} \begin{bmatrix} -1 + \mathbf{i} \\ -1 + \mathbf{i} \end{bmatrix} \right) = \frac{1}{3} (2^{n-r} (2^{2r} + 1) S_\alpha - 2(-1)^{n-r} S_\beta) \end{aligned}$$

where the spinors S_α and S_β are $S_\alpha = \begin{bmatrix} 8 + \mathbf{i} \\ 2 + 4\mathbf{i} \end{bmatrix}$ and $S_\beta = (-1 + \mathbf{i}) \begin{bmatrix} 1 \\ 1 \end{bmatrix}$.

iv) Similarly, we can easily obtain the equation

$$SJ_{n+r} - SJ_{n-r} = \frac{1}{3} 2^{n-r} (2^{2r} - 1) \begin{bmatrix} 8 + \mathbf{i} \\ 2 + 4\mathbf{i} \end{bmatrix} = \frac{1}{3} 2^{n-r} (2^{2r} - 1) S_\alpha$$

where we have $J_{n+r} - J_{n-r} = \frac{1}{3} 2^{n-r} (2^{2r} - 1)$ in [4].

Similar to Theorem 6, we can easily give the following demonstrable theorem.

Theorem 7. Let n th, $(n+1)$ th, $(n+r)$ th, and $(n-r)$ th Jacobsthal-Lucas spinors are SJL_n , SJL_{n+1} , SJL_{n+r} , and SJL_{n-r} , respectively. In this case, for $n \geq 1$, $r \geq 1$ there are the following relations;

- i) $SJL_{n+1} + SJL_n = 3 \cdot 2^n S_\alpha$,
- ii) $SJL_{n+1} - SJL_n = 2^n S_\alpha - 2(-1)^n S_\beta$,
- iii) $SJL_{n+r} + SJL_{n-r} = 2^{n-r} (2^{2r} + 1) S_\alpha + 2(-1)^{n-r} S_\beta$,
- iv) $SJL_{n+r} - SJL_{n-r} = 2^{n-r} (2^{2r} - 1) S_\alpha$

where the spinors S_α and S_β are $S_\alpha = \begin{bmatrix} \alpha^3 + \mathbf{i} \\ \alpha + \mathbf{i}\alpha^2 \end{bmatrix} = \begin{bmatrix} 8 + \mathbf{i} \\ 2 + 4\mathbf{i} \end{bmatrix}$ and

$$S_\beta = \begin{bmatrix} \beta^3 + \mathbf{i} \\ \beta + \mathbf{i}\beta^2 \end{bmatrix} = \begin{bmatrix} -1 + \mathbf{i} \\ -1 + \mathbf{i} \end{bmatrix} = (-1 + \mathbf{i}) \begin{bmatrix} 1 \\ 1 \end{bmatrix}, \text{ respectively.}$$

Theorem 8. Let n th Jacobsthal and Jacobsthal-Lucas spinors be SJ_n and SJL_n , respectively. So, the relationships between Jacobsthal and Jacobsthal-Lucas spinors are

- i) $SJ_n + SJL_n = 2SJ_{n+1}$,
- ii) $SJ_{n+1} + 2SJ_{n-1} = SJL_n$,
- iii) $3SJ_n + SJL_n = 2^{n+1} S_\alpha$

where $S_\alpha = \begin{bmatrix} 8 + \mathbf{i} \\ 2 + 4\mathbf{i} \end{bmatrix}$.

Proof: Assume that n th Jacobsthal and Jacobsthal-Lucas spinors are SJ_n and SJL_n , respectively. Now, we can give proofs.

i) We demonstrate the summation of Jacobsthal and Jacobsthal-Lucas spinors $SJ_n + SJL_n$. In this case, we obtain

$$SJ_n + SJL_n = \begin{bmatrix} J_{n+3} + \mathbf{i}J_n \\ J_{n+1} + \mathbf{i}J_{n+2} \end{bmatrix} + \begin{bmatrix} JL_{n+3} + \mathbf{i}JL_n \\ JL_{n+1} + \mathbf{i}JL_{n+2} \end{bmatrix} = \begin{bmatrix} J_{n+3} + JL_{n+3} + \mathbf{i}(J_n + JL_n) \\ J_{n+1} + JL_{n+1} + \mathbf{i}(J_{n+2} + JL_{n+2}) \end{bmatrix}.$$

On the other hand, we know that $J_n + JL_n = 2J_{n+1}$ for Jacobsthal and Jacobsthal-Lucas numbers from [4]. Consequently, we get

$$SJ_n + SJL_n = \begin{bmatrix} 2J_{n+4} + \mathbf{i}2J_{n+1} \\ 2J_{n+2} + \mathbf{i}2J_{n+3} \end{bmatrix} = 2SJ_{n+1}.$$

This completes the proof.

ii) $(n-1)$ th, $(n+1)$ th Jacobsthal spinors are SJ_{n-1} , SJ_{n+1} and n th Jacobsthal-Lucas spinor is SJL_n . Therefore, we have

$$SJ_{n+1} + 2SJ_{n-1} = \begin{bmatrix} J_{n+4} + 2J_{n+2} + \mathbf{i}(J_{n+1} + 2J_{n-1}) \\ J_{n+2} + 2J_n + \mathbf{i}(J_{n+3} + 2J_{n+1}) \end{bmatrix} = \begin{bmatrix} JL_{n+3} + \mathbf{i}JL_n \\ JL_{n+1} + \mathbf{i}JL_{n+2} \end{bmatrix} = SJL_n$$

where we use the equation $J_{n+1} + 2J_{n-1} = JL_n$ in [4].

iii) Similarly, we can easily obtain that

$$3SJ_n + SJL_n = \begin{bmatrix} 3J_{n+3} + JL_{n+3} + \mathbf{i}(3J_n + JL_n) \\ 3J_{n+1} + JL_{n+1} + \mathbf{i}(3J_{n+2} + JL_{n+2}) \end{bmatrix} = \begin{bmatrix} 2^{n+4} + \mathbf{i}2^{n+1} \\ 2^{n+2} + \mathbf{i}2^{n+3} \end{bmatrix} = 2^{n+1} \begin{bmatrix} 8 + 2\mathbf{i} \\ 2 + 4\mathbf{i} \end{bmatrix} = 2^{n+1} S_\alpha.$$

We have the equation $3J_n + JL_n = 2^{n+1}$ from [4] in here. The proof is completed.

Theorem 9. Assume that n th Jacobsthal and Jacobsthal-Lucas spinors are SJ_n and SJL_n , respectively. Therefore, Binet Formulas for these spinors are the following equations.

i) Binet formula for Jacobsthal spinors is

$$SJ_n = \frac{1}{3} \left(2^n S_\alpha - (-1)^n S_\beta \right), \quad (6)$$

ii) Binet formula for Jacobsthal-Lucas spinors is

$$SJL_n = 2^n S_\alpha + (-1)^n S_\beta \quad (7)$$

where $\alpha = 2$, $\beta = -1$ are the roots of characteristic equation $x^2 - x - 2 = 0$ and

$$S_\alpha = \begin{bmatrix} \alpha^3 + \mathbf{i} \\ \alpha + \mathbf{i}\alpha^2 \end{bmatrix} = \begin{bmatrix} 8 + \mathbf{i} \\ 2 + 4\mathbf{i} \end{bmatrix} \text{ and } S_\beta = \begin{bmatrix} \beta^3 + \mathbf{i} \\ \beta + \mathbf{i}\beta^2 \end{bmatrix} = \begin{bmatrix} -1 + \mathbf{i} \\ -1 + \mathbf{i} \end{bmatrix} = (-1 + \mathbf{i}) \begin{bmatrix} 1 \\ 1 \end{bmatrix}.$$

Proof:

i) We know that Binet formula for the Jacobsthal number sequence is $J_n = \frac{2^n - (-1)^n}{3}$ in

[4]. Therefore, if we write the last equation in the n th Jacobsthal spinor we obtain

$$\begin{aligned} SJ_n &= \begin{bmatrix} J_{n+3} + \mathbf{i}J_n \\ J_{n+1} + \mathbf{i}J_{n+2} \end{bmatrix} = \begin{bmatrix} \frac{2^{n+3} - (-1)^{n+3}}{3} + \mathbf{i}\frac{2^n - (-1)^n}{3} \\ \frac{2^{n+1} - (-1)^{n+1}}{3} + \mathbf{i}\frac{2^{n+2} - (-1)^{n+2}}{3} \end{bmatrix} = \frac{1}{3} \left(\begin{bmatrix} 2^{n+3} + \mathbf{i}2^n \\ 2^{n+1} + \mathbf{i}2^{n+2} \end{bmatrix} - \begin{bmatrix} (-1)^{n+3} + \mathbf{i}(-1)^n \\ (-1)^{n+1} + \mathbf{i}(-1)^{n+2} \end{bmatrix} \right) \\ &= \frac{1}{3} \left(2^n \begin{bmatrix} 8 + \mathbf{i} \\ 2 + 4\mathbf{i} \end{bmatrix} - (-1)^n (-1 + \mathbf{i}) \begin{bmatrix} 1 \\ 1 \end{bmatrix} \right) \end{aligned}$$

or

$$SJ_n = \frac{1}{3} \left(2^n S_\alpha - (-1)^n S_\beta \right)$$

where $S_\alpha = \begin{bmatrix} 8 + \mathbf{i} \\ 2 + 4\mathbf{i} \end{bmatrix}$ and $S_\beta = (-1 + \mathbf{i}) \begin{bmatrix} 1 \\ 1 \end{bmatrix}$.

ii) Now, we give the Binet formula for Jacobsthal-Lucas spinors. We know that the Binet formula for Jacobsthal-Lucas number sequence is $JL_n = 2^n + (-1)^n$ in [4]. In this case, we can obtain

$$\begin{aligned} SJL_n &= \begin{bmatrix} JL_{n+3} + \mathbf{i}JL_n \\ JL_{n+1} + \mathbf{i}JL_{n+2} \end{bmatrix} = \begin{bmatrix} 2^{n+3} + (-1)^{n+3} + \mathbf{i}(2^n + (-1)^n) \\ 2^{n+1} + (-1)^{n+1} + \mathbf{i}(2^{n+2} + (-1)^{n+2}) \end{bmatrix} = \begin{bmatrix} 2^{n+3} + \mathbf{i}2^n \\ 2^{n+1} + \mathbf{i}2^{n+2} \end{bmatrix} + \begin{bmatrix} (-1)^{n+3} + \mathbf{i}(-1)^n \\ (-1)^{n+1} + \mathbf{i}(-1)^{n+2} \end{bmatrix} \\ &= 2^n \begin{bmatrix} 8 + \mathbf{i} \\ 2 + 4\mathbf{i} \end{bmatrix} + (-1)^n (-1 + \mathbf{i}) \begin{bmatrix} 1 \\ 1 \end{bmatrix}. \end{aligned}$$

or

$$SJL_n = 2^n S_\alpha + (-1)^n S_\beta$$

where $S_\alpha = \begin{bmatrix} 8 + \mathbf{i} \\ 2 + 4\mathbf{i} \end{bmatrix}$ and $S_\beta = (-1 + \mathbf{i}) \begin{bmatrix} 1 \\ 1 \end{bmatrix}$.

Theorem 10. Let n th Jacobsthal, Jacobsthal-Lucas spinors be SJ_n , SJL_n and fundamental Jacobsthal, Jacobsthal-Lucas spinor matrices (left Hamilton Jacobsthal, Jacobsthal-Lucas spinor matrices) be $(SJ_n)_L$, $(SJL_n)_L$, respectively. Therefore, for fundamental Jacobsthal and Jacobsthal-Lucas spinor matrices there are the following equations;

$$i) (SJ_n)_L = \frac{1}{3} \left(2^n (S_\alpha)_L - (-1)^n (S_\beta)_L \right), \quad (8)$$

and

$$ii) (SJL_n)_L = 2^n (S_\alpha)_L + (-1)^n (S_\beta)_L \quad (9)$$

where $(S_\alpha)_L = \begin{bmatrix} 1-8\mathbf{i} & -4-2\mathbf{i} \\ 4-2\mathbf{i} & 1+8\mathbf{i} \end{bmatrix}$ and $(S_\beta)_L = \begin{bmatrix} 1+\mathbf{i} & -1+\mathbf{i} \\ 1+\mathbf{i} & 1-\mathbf{i} \end{bmatrix}$ are left Hamilton spinor matrices (fundamental spinor matrices) corresponding to the spinors S_α and S_β , respectively.

Proof:

i) We assume n th Jacobsthal spinor SJ_n . If we use the equation (4), then we get

$$(SJ_n)_L = \begin{bmatrix} J_n - \mathbf{i}J_{n+3} & -J_{n+2} - \mathbf{i}J_{n+1} \\ J_{n+2} - \mathbf{i}J_{n+1} & J_n + \mathbf{i}J_{n+3} \end{bmatrix}.$$

Now, we use Binet formula for Jacobsthal numbers $J_n = \frac{2^n - (-1)^n}{3}$ in [4]. Therefore, we have

$$\begin{aligned} (SJ_n)_L &= \frac{1}{3} \begin{bmatrix} 2^n - (-1)^n - \mathbf{i}(2^{n+3} - (-1)^{n+3}) & -(2^{n+2} - (-1)^{n+2}) - \mathbf{i}(2^{n+1} - (-1)^{n+1}) \\ 2^{n+2} - (-1)^{n+2} - \mathbf{i}(2^{n+1} - (-1)^{n+1}) & 2^n - (-1)^n + \mathbf{i}(2^{n+3} - (-1)^{n+3}) \end{bmatrix} \\ &= \frac{1}{3} \left(2^n \begin{bmatrix} 1-8\mathbf{i} & -4-2\mathbf{i} \\ 4-2\mathbf{i} & 1+8\mathbf{i} \end{bmatrix} - (-1)^n \begin{bmatrix} 1+\mathbf{i} & -1+\mathbf{i} \\ 1+\mathbf{i} & 1-\mathbf{i} \end{bmatrix} \right). \end{aligned}$$

If we use again the equation (4), then we obtain

$$(SJ_n)_L = \frac{1}{3} \left(2^n (S_\alpha)_L - (-1)^n (S_\beta)_L \right)$$

where $(S_\alpha)_L = \begin{bmatrix} 1-8\mathbf{i} & -4-2\mathbf{i} \\ 4-2\mathbf{i} & 1+8\mathbf{i} \end{bmatrix}$ and $(S_\beta)_L = \begin{bmatrix} 1+\mathbf{i} & -1+\mathbf{i} \\ 1+\mathbf{i} & 1-\mathbf{i} \end{bmatrix}$.

ii) Let n th Jacobsthal-Lucas spinor SJL_n . If we use the equation (4) for Jacobsthal-Lucas spinor, then we obtain $(SJL_n)_L = \begin{bmatrix} JL_n - \mathbf{i}JL_{n+3} & -JL_{n+2} - \mathbf{i}JL_{n+1} \\ JL_{n+2} - \mathbf{i}JL_{n+1} & JL_n + \mathbf{i}JL_{n+3} \end{bmatrix}$. On the other hand, we

use Binet formula for Jacobsthal-Lucas numbers $JL_n = 2^n + (-1)^n$ in [4]. So, we have

$$\begin{aligned} (SJL_n)_L &= \begin{bmatrix} 2^n + (-1)^n - \mathbf{i}(2^{n+3} + (-1)^{n+3}) & -(2^{n+2} + (-1)^{n+2}) - \mathbf{i}(2^{n+1} + (-1)^{n+1}) \\ 2^{n+2} + (-1)^{n+2} - \mathbf{i}(2^{n+1} + (-1)^{n+1}) & 2^n + (-1)^n + \mathbf{i}(2^{n+3} + (-1)^{n+3}) \end{bmatrix} \\ &= 2^n \begin{bmatrix} 1-8\mathbf{i} & -4-2\mathbf{i} \\ 4-2\mathbf{i} & 1+8\mathbf{i} \end{bmatrix} + (-1)^n \begin{bmatrix} 1+\mathbf{i} & -1+\mathbf{i} \\ 1+\mathbf{i} & 1-\mathbf{i} \end{bmatrix}. \end{aligned}$$

If we use the equation (4), then we get $(S_\alpha)_L = \begin{bmatrix} 1-8\mathbf{i} & -4-2\mathbf{i} \\ 4-2\mathbf{i} & 1+8\mathbf{i} \end{bmatrix}$ and $(S_\beta)_L = \begin{bmatrix} 1+\mathbf{i} & -1+\mathbf{i} \\ 1+\mathbf{i} & 1-\mathbf{i} \end{bmatrix}$

which are left Hamilton spinor matrices corresponding to the spinors S_α and S_β , respectively.

Consequently, we find

$$(SJL_n)_L = 2^n (S_\alpha)_L + (-1)^n (S_\beta)_L.$$

Now, we express the Cassini Formula for Jacobsthal and Jacobsthal-Lucas spinors.

Theorem 11. Assume that $(n-1)$ th, n th and $(n+1)$ th Jacobsthal spinors are SJ_{n-1} , SJ_n and SJ_{n+1} . In this case, Cassini formula for Jacobsthal spinors is

$$(SJ_{n-1})_L SJ_{n+1} - (SJ_n)_L SJ_n = -(-2)^{n-1} (5 + 7\mathbf{i}) \begin{bmatrix} 1 \\ 1 \end{bmatrix}$$

and considering $(n-1)$ th, n th and $(n+1)$ th Jacobsthal-Lucas spinors are SJL_{n-1} , SJL_n and SJL_{n+1} for Jacobsthal-Lucas spinors the similar formula is

$$(SJL_{n-1})_L SJL_{n+1} - (SJL_n)_L SJL_n = 9(-2)^{n-1} (5 + 7\mathbf{i}) \begin{bmatrix} 1 \\ 1 \end{bmatrix}$$

for $n \geq 1$.

Proof: Firstly, we give Cassini formula for Jacobsthal spinors. Jacobsthal spinor product corresponding to the product of Jacobsthal quaternions $JQ_{n-1}JQ_{n+1} - (JQ_n)^2$ is $(SJ_{n-1})_L SJ_{n+1} - (SJ_n)_L SJ_n$. In this case, if we use the Binet formula $SJ_n = \frac{1}{3}(2^n S_\alpha - (-1)^n S_\beta)$ in the equation (6) and the equation (8) for Jacobsthal spinors, then we get

$$(SJ_{n-1})_L SJ_{n+1} - (SJ_n)_L SJ_n = \frac{1}{9} \left(\begin{aligned} & \left(-2^{n-1} (-1)^{n+1} + 2^n (-1)^n \right) (S_\alpha)_L S_\beta \\ & + \left(-2^{n+1} (-1)^{n-1} + 2^n (-1)^n \right) (S_\beta)_L S_\alpha \end{aligned} \right). \quad (10)$$

If we make necessary arrangements in the last equation, then we have

$$(SJ_{n-1})_L SJ_{n+1} - (SJ_n)_L SJ_n = -\frac{1}{3} (-2)^{n-1} \left((S_\alpha)_L S_\beta + 2(S_\beta)_L S_\alpha \right).$$

Now, we calculate the spinor product $(S_\alpha)_L S_\beta + 2(S_\beta)_L S_\alpha$. Therefore, we obtain

$$\begin{aligned} (S_\alpha)_L S_\beta + 2(S_\beta)_L S_\alpha &= \begin{bmatrix} 1-8\mathbf{i} & -4-2\mathbf{i} \\ 4-2\mathbf{i} & 1+8\mathbf{i} \end{bmatrix} \begin{bmatrix} -1+\mathbf{i} \\ -1+\mathbf{i} \end{bmatrix} + 2 \begin{bmatrix} 1+\mathbf{i} & -1+\mathbf{i} \\ 1+\mathbf{i} & 1-\mathbf{i} \end{bmatrix} \begin{bmatrix} 8+\mathbf{i} \\ 2+4\mathbf{i} \end{bmatrix} \\ &= \begin{bmatrix} 13+7\mathbf{i} \\ -11-\mathbf{i} \end{bmatrix} + 2 \begin{bmatrix} 1+7\mathbf{i} \\ 13+11\mathbf{i} \end{bmatrix} = \begin{bmatrix} 15+21\mathbf{i} \\ 15+21\mathbf{i} \end{bmatrix}. \end{aligned} \quad (11)$$

Considering the equations (10) and (11) consequently, we obtain

$$(SJ_{n-1})_L SJ_{n+1} - (SJ_n)_L SJ_n = -(-2)^{n-1} (5+7\mathbf{i}) \begin{bmatrix} 1 \\ 1 \end{bmatrix}.$$

Similarly, for Jacobsthal-Lucas spinors considering Binet formula $(SJL_n)_L = 2^n (S_\alpha)_L + (-1)^n (S_\beta)_L$ in the equation (7) and $(SJL_n)_L = 2^n (S_\alpha)_L + (-1)^n (S_\beta)_L$ in the equation (9), we have

$$\begin{aligned} (SJL_{n-1})_L SJL_{n+1} - (SJL_n)_L SJL_n &= \begin{pmatrix} \left(2^{n-1} (S_\alpha)_L + (-1)^{n-1} (S_\beta)_L \right) \left(2^{n+1} S_\alpha + (-1)^{n+1} S_\beta \right) \\ - \left(2^n (S_\alpha)_L + (-1)^n (S_\beta)_L \right) \left(2^n S_\alpha + (-1)^n S_\beta \right) \end{pmatrix} \\ &= 3(-2)^{n-1} \left((S_\alpha)_L S_\beta + 2(S_\beta)_L S_\alpha \right). \end{aligned}$$

If we use the equation (11) in the last equation, consequently we have

$$(SJL_{n-1})_L SJL_{n+1} - (SJL_n)_L SJL_n = 9(-2)^{n-1} (5 + 7\mathbf{i}) \begin{bmatrix} 1 \\ 1 \end{bmatrix}.$$

Theorem 12. The generating function for Jacobsthal spinors is

$$G_{SJ}(t) = \frac{1}{1-t-2t^2} \begin{bmatrix} 3+2t+\mathbf{i}t \\ 1+\mathbf{i}(1+2t) \end{bmatrix}$$

and the generating function for Jacobsthal-Lucas spinors is

$$G_{SJL}(t) = \frac{1}{1-t-2t^2} \begin{bmatrix} 7+10t+\mathbf{i}(2-t) \\ 1+4t+\mathbf{i}(5+2t) \end{bmatrix}.$$

Proof: We take n th Jacobsthal spinor as SJ_n . Therefore, for n th Jacobsthal spinor the generating function is calculated with the aid of the equation $G_{SJ}(t) = \sum_{n=0}^{\infty} SJ_n t^n$. In this case,

using $G_{SJ}(t)$, $tG_{SJ}(t)$ and $2t^2G_{SJ}(t)$ we obtain that

$$\begin{aligned} G_{SJ}(t) &= SJ_0 + SJ_1 t + SJ_2 t^2 + SJ_3 t^3 + SJ_4 t^4 + SJ_5 t^5 + \dots \\ -tG_{SJ}(t) &= -SJ_0 t - SJ_1 t^2 - SJ_2 t^3 - SJ_3 t^4 - SJ_4 t^5 - SJ_5 t^6 + \dots \\ -2t^2G_{SJ}(t) &= -2SJ_0 t^2 - 2SJ_1 t^3 - 2SJ_2 t^4 - 2SJ_3 t^5 - 2SJ_4 t^6 - 2SJ_5 t^7 + \dots \end{aligned}$$

and

$$G_{SJ}(t) = \frac{1}{(1-t-2t^2)} (SJ_0 + (SJ_1 - SJ_0)t)$$

where

$$SJ_0 + (SJ_1 - 2SJ_0)t = \begin{bmatrix} 3 \\ 1+\mathbf{i} \end{bmatrix} + \left(\begin{bmatrix} 5+\mathbf{i} \\ 1+3\mathbf{i} \end{bmatrix} - \begin{bmatrix} 3 \\ 1+\mathbf{i} \end{bmatrix} \right) t = \begin{bmatrix} 3+2t+\mathbf{i}t \\ 1+\mathbf{i}(1+2t) \end{bmatrix}.$$

Consequently, we get

$$G_{SJ}(t) = \frac{1}{1-t-2t^2} \begin{bmatrix} 3+2t+\mathbf{i}t \\ 1+\mathbf{i}(1+2t) \end{bmatrix}.$$

Now, we calculate the generating function for Jacobsthal-Lucas spinors. Therefore, if

we consider the function $G_{SJL}(t) = \sum_{n=0}^{\infty} SJL_n t^n$, we have

$$G_{SJL}(t) = \frac{1}{(1-t-2t^2)} (SJL_0 + (SJL_1 - SJL_0)t)$$

considering $G_{SJL}(t)$, $tG_{SJL}(t)$ and $2t^2G_{SJL}(t)$. Finally, we obtain

$$G_{SJL}(t) = \frac{1}{1-t-2t^2} \begin{bmatrix} 7+10t+\mathbf{i}(2-t) \\ 1+4t+\mathbf{i}(5+2t) \end{bmatrix}.$$

This completes the proof.

Theorem 13. Assume that $(-n)$ th Jacobsthal and Jacobsthal-Lucas spinors are SJ_{-n} and SJL_{-n} . In this case these spinors are calculated as follows;

for Jacobsthal spinors

$$SJ_{-n} = \left(-\frac{1}{2}\right)^n \begin{bmatrix} 8J_{n-3} - \mathbf{i}J_n \\ 2J_{n-1} - \mathbf{i}4J_{n-2} \end{bmatrix},$$

for Jacobsthal-Lucas spinors

$$SJL_{-n} = -\left(-\frac{1}{2}\right)^n \begin{bmatrix} 8JL_{n-3} - \mathbf{i}JL_n \\ 2JL_{n-1} - \mathbf{i}4JL_{n-2} \end{bmatrix}.$$

Proof: We know that the Jacobsthal spinor $SJ_n = \begin{bmatrix} J_{n+3} + \mathbf{i}J_n \\ J_{n+1} + \mathbf{i}J_{n+2} \end{bmatrix}$ with the aid of the equation (5).

In this case, for $(-n)$ th the Jacobsthal spinor we can write

$$SJ_{-n} = \begin{bmatrix} J_{-n+3} + \mathbf{i}J_{-n} \\ J_{-n+1} + \mathbf{i}J_{-n+2} \end{bmatrix}.$$

On the other hand, the equation for negative subscript $(-n)$ th Jacobsthal number is known as

$J_{-n} = \frac{(-1)^{n+1}}{2^n} J_n$. Therefore, we obtain

$$SJ_{-n} = \begin{bmatrix} \frac{(-1)^{n-2}}{2^{n-3}} J_{n-3} + \mathbf{i} \frac{(-1)^{n+1}}{2^n} J_n \\ \frac{(-1)^n}{2^{n-1}} J_{n-1} + \mathbf{i} \frac{(-1)^{n-1}}{2^{n-2}} J_{n-2} \end{bmatrix} = \frac{(-1)^{n+1}}{2^n} \begin{bmatrix} -8J_{n-3} + \mathbf{i}J_n \\ -2J_{n-1} + \mathbf{i}4J_{n-2} \end{bmatrix}$$

and consequently

$$SJ_{-n} = \left(-\frac{1}{2}\right)^n \begin{bmatrix} 8J_{n-3} - \mathbf{i}J_n \\ 2J_{n-1} - \mathbf{i}4J_{n-2} \end{bmatrix}.$$

Now, we calculate the Jacobsthal-Lucas spinor SJL_{-n} for negative subscript $(-n)$ th. We

know that the Jacobsthal-Lucas spinor $SJL_n = \begin{bmatrix} JL_{n+3} + \mathbf{i}JL_n \\ JL_{n+1} + \mathbf{i}JL_{n+2} \end{bmatrix}$ from the equation (5). So, for

$(-n)$ th the Jacobsthal-Lucas spinor we can write

$$SJL_{-n} = \begin{bmatrix} JL_{-n+3} + \mathbf{i}JL_{-n} \\ JL_{-n+1} + \mathbf{i}JL_{-n+2} \end{bmatrix}.$$

On the other hand, the equation for negative subscript $(-n)$ th Jacobsthal-Lucas number is

known as $JL_{-n} = \frac{(-1)^n}{2^n} JL_n$. Consequently, we get

$$SJL_{-n} = \begin{bmatrix} \frac{(-1)^{n-3}}{2^{n-3}} JL_{n-3} + \mathbf{i} \frac{(-1)^n}{2^n} JL_n \\ \frac{(-1)^{n-1}}{2^{n-1}} JL_{n-1} + \mathbf{i} \frac{(-1)^{n-2}}{2^{n-2}} JL_{n-2} \end{bmatrix} = -\left(-\frac{1}{2}\right)^n \begin{bmatrix} 8JL_{n-3} - \mathbf{i}JL_n \\ 2JL_{n-1} - \mathbf{i}4JL_{n-2} \end{bmatrix}.$$

Theorem 14. Let n th Jacobsthal spinor be SJ_n . The summation formulas for Jacobsthal spinors are the following options;

$$\begin{aligned} i) \sum_{s=1}^n SJ_s &= \frac{1}{2} [SJ_{n+2} - SJ_2], \\ ii) \sum_{s=0}^p SJ_{n+s} &= \frac{1}{2} [SJ_{n+p+2} - SJ_{n+1}]. \end{aligned}$$

Proof:

i) We know that for Jacobsthal spinors the Binet formula is

$$\sum_{s=1}^n SJ_s = \sum_{s=1}^n \left(\frac{1}{3} \left(2^n S_\alpha - (-1)^n S_\beta \right) \right) = \frac{1}{3} \left(\left(\sum_{s=1}^n 2^n \right) S_\alpha - \left(\sum_{s=1}^n (-1)^n \right) S_\beta \right).$$

On the other hand, we know that there is the equation $\sum_{s=1}^n x^s = \frac{x - x^{n+1}}{1 - x}$ for geometric sequences.

Then we have

$$\sum_{s=1}^n SJ_s = \frac{1}{3} \left(\left(\frac{2 - 2^{n+1}}{1 - 2} \right) S_\alpha - \left(\frac{-1 - (-1)^{n+1}}{1 - (-1)} \right) S_\beta \right) = \frac{1}{6} \left((-4 + 2^{n+2}) S_\alpha + (1 + (-1)^{n+1}) S_\beta \right).$$

Now, we make necessary arrangements and use Binet formula for Jacobsthal spinors in the equation (6). Therefore we get

$$\sum_{s=1}^n SJ_s = \frac{1}{6} \left(-4S_\alpha + 2^{n+2} S_\alpha + S_\beta + (-1)^{n+1} S_\beta \right) = \frac{1}{2} \left(-\frac{1}{3} (2^2 S_\alpha - S_\beta) + \frac{1}{3} (2^{n+2} S_\alpha - (-1)^{n+2} S_\beta) \right)$$

and consequently

$$\sum_{s=1}^n SJ_s = \frac{1}{2} (SJ_{n+2} - SJ_2).$$

ii) Now, we find the summation formulas for Jacobsthal spinors with subscript $(n + s)$ th.

With the aid of the equation (6) is

$$\sum_{s=0}^p SJ_{n+s} = \sum_{s=1}^n \left(\frac{1}{3} \left(2^{n+s} S_\alpha - (-1)^{n+s} S_\beta \right) \right) = \frac{1}{3} \left(\left(\sum_{s=1}^n 2^{n+s} \right) S_\alpha - \left(\sum_{s=1}^n (-1)^{n+s} \right) S_\beta \right).$$

Moreover, there is the equation $\sum_{s=0}^n x^{n+s} = \frac{x^n - x^{n+p+1}}{1 - x}$ for geometric sequences. Therefore, we

have

$$\sum_{s=0}^p SJ_{n+s} = \frac{1}{3} \left(\left(\frac{2^n - 2^{n+p+1}}{1 - 2} \right) S_\alpha - \left(\frac{(-1)^n - (-1)^{n+p+1}}{1 - (-1)} \right) S_\beta \right) = \frac{1}{6} \left((-2^{n+1} + 2^{n+p+2}) S_\alpha - ((-1)^n - (-1)^{n+p+1}) S_\beta \right).$$

If we make necessary arrangements and use Binet formula for Jacobsthal spinors in the equation (6), then we get

$$\sum_{s=0}^p SJ_{n+s} = \frac{1}{2} \left(-\frac{1}{3} (2^{n+1} S_\alpha - (-1)^{n+1} S_\beta) + \frac{1}{3} (2^{n+p+2} S_\alpha - (-1)^{n+p+2} S_\beta) \right)$$

and consequently

$$\sum_{s=0}^p SJ_{n+s} = \frac{1}{2} [SJP_{n+p+2} - SJ_{n+1}].$$

Similar to Theorem 13, we can express the following demonstrable theorem.

Theorem 14. Assume that n th Jacobsthal-Lucas spinor be SJL_n . The summation formulas for Jacobsthal-Lucas spinors are the following equations;

$$i) \sum_{s=1}^n SJL_s = \frac{1}{2} [SJL_{n+2} - SJL_2],$$

$$ii) \sum_{s=0}^p SJL_{n+s} = \frac{1}{2} [SJL_{n+p+2} - SJL_{n+1}].$$

References

- [1] Koshy, T., *Fibonacci and Lucas numbers with applications*, John Wiley and Sons, Proc. New York-Toronto, 2001.
- [2] Hoggatt, J.R., Verner, E., *Fibonacci and Lucas numbers*, The Fibonacci Association, California, 1979.
- [3] Basin, S.L., Hoggatt, V.E., *A primer on the Fibonacci sequence*, The Fibonacci Quaterly, 2, 61-68, 1963.
- [4] Horadam, A.F., *Jacobsthal representation numbers*, Fibonacci Quart., 34, 40-54, 1996.
- [5] Horadam, A.F., *Pell identities*, Fibonacci Quart., 9, 245 – 252, 1971.
- [6] Horadam, A.F., *Applications of modified Pell numbers to representations*, Ulam Quaterly, 3(1), 1994.
- [7] Horadam, A.F., *Complex Fibonacci numbers and Fibonacci quaternions*, Amer. Math. Monthly, 70(3), 289-291, 1963.
- [8] Horadam, A.F., *Quaternion recurrence relations*, Ulam Quaterly, 2(2), 23-33, 1993.
- [9] Horadam, A.F., Filipponi, P., *Real Pell and Pell-Lucas numbers with real subscripts*, The Fib. Quart., 33(5), 398-406, 1995.
- [10] Cerin, Z., Gianella, G.M., *On sums of Pell numbers*, Acc. Sc. Torino-Atti Sc. Fis., 141, 23-31, 2007.
- [11] Serkland, C.E., *The Pell sequence and some generalizations*, Master's Thesis, San Jose State University, San Jose, California, 1972.
- [12] Daşdemir, A., *A study on the Jacobsthal and Jacobsthal-Lucas numbers*, DUFED, 3(1), 13-18, 2014.
- [13] Szyal-Lianna, A., Wloch, I., *A note on Jacobsthal quaternions*, Adv. in Appl. Cliff. Algebr., 26(1), 441-447, 2016.

- [14] Torunbalcı Aydın, F., Yüce, S., *A new approach to Jacobsthal quaternions*, *Filomat* 31(18), 5567-5579, 2017.
- [15] Halıcı, S., *On bicomplex Jacobsthal-Lucas numbers*, *Journal of Mathematical Sciences and Modelling*, 3(3), 139-143, 2020.
- [16] Çelik, S., Durukan, İ., Özkan, E., *New recurrences on Pell numbers, Pell-Lucas numbers, Jacobsthal numbers and Jacobsthal-Lucas numbers*, *Chaos Solitons Fractals*, 150, 111173, 2021.
- [17] Arslan, H., *On complex Gaussian Jacobsthal and Jacobsthal-Lucas quaternions*, *Cumhuriyet Sci. J.*, 41(1), 1-10, 2020.
- [18] Özkan, E., Uysal, M., *On quaternions with higher order Jacobsthal numbers components*, *GU J Sci.*, 36(1), 336-347, 2023.
- [19] Bród, D., Szytal-Liana, A., *On $J(r, n)$ -Jacobsthal quaternions*, *Pure and Applied Mathematics Quarterly*, 14(3-4), 579-590, 2018.
- [20] Özkan, E., Taştan, M., *A New Families of Gauss k -Jacobsthal Numbers and Gauss k -Jacobsthal-Lucas Numbers and Their Polynomials*, *Journal of Science and Arts*, 4(53), 893-908, 2020.
- [21] Özkan, E., Uysal, M., *On Hyperbolic k -Jacobsthal and k -Jacobsthal-Lucas Octonions*, *Notes on Number Theory and Discrete Mathematics*, 28(2), 318-330, 2022.
- [22] Cartan, E., *The theory of spinors*, Dover Publications, New York, 1966.
- [23] Vivarelli, M.D., *Development of spinors descriptions of rotational mechanics from Euler's rigid body displacement theorem*, *Celestial Mechanics*, 32, 193-207, 1984.
- [24] Torres Del Castillo, G.F., Barrales, G.S., *Spinor formulation of the differential geometry of curves*, *Revista Colombiana de Matematicas*, 38, 27-34, 2004.
- [25] Kişi, İ., Tosun, M., *Spinor Darboux equations of curves in Euclidean 3-space*, *Math. Morav.*, 19(1), 87-93, 2015.
- [26] Ünal, D., Kişi, İ., Tosun, M., *Spinor Bishop equation of curves in Euclidean 3-space*, *Adv. in Appl. Cliff. Algebr.*, 23(3), 757-765, 2013.
- [27] Erişir, T., Kardağ, N.C., *Spinor representations of involute evolute curves in E^3* , *Fundam. J. Math. Appl.*, 2(2), 148-155, 2019.
- [28] Erişir, T., *On spinor construction of Bertrand curves*, *AIMS Mathematics*, 6(4), 3583-3591, 2021.
- [29] Erişir, T., İsabeyoğlu, Z., *The spinor expressions of Mannheim curves in Euclidean 3-space*, *Int. Electron. J. Geom.*, 16(1), 111-121, 2023.
- [30] Erişir, T., Köse Öztaş, H., *Spinor equations of successor curves*, *Univ. J. Math. Appl.*, 5(1), 32-41, 2022.
- [31] Şenyurt, S., Çalışkan, A., *Spinor Formulation of Sabban Frame of Curve on S^2* , *Pure Mathematical Sciences*, 4(1), 37-42, 2015.
- [32] Okuyucu, O. Z., Yıldız, Ö. G., and Tosun, M., *Spinor Frenet equations in three dimensional Lie Groups*, *Adv. in Appl. Cliff. Algebr.*, 26, 1341-1348, 2016.
- [33] Ketenci, Z., Erişir, T., Güngör, M.A., *A construction of hyperbolic spinors according to Frenet frame in Minkowski space*, *Journal of Dynamical Systems and Geometric Theories*, 13(2), 179-193, 2015.

[34] Balcı, Y., Erişir, T., Güngör, M.A., *Hyperbolic spinor Darboux equations of spacelike curves in Minkowski 3-space*, Journal of the Chungcheong Mathematical Society, 28(4), 525-535, 2015.

[35] Erişir, T., Güngör, M.A., Tosun, M., *Geometry of the hyperbolic spinors corresponding to alternative frame*, Adv. in Appl. Cliff. Algebr., 25(4), 799-810, 2015.

[36] Tarakçıoğlu, M., Erişir, T., Güngör, M.A., Tosun, M., *The hyperbolic spinor representation of transformations in R_1^3 by means of split quaternions*, Adv. in Appl. Cliff. Algebr., 28(1), 26, 2018.

[37] Erişir, T., Güngör, M.A., *Fibonacci spinors*, International Journal of Geometric Methods in Modern Physics, 17(4), 2050065, 2020.

[38] Hacısalihoğlu, H.H., *Geometry of motion and theory of quaternions*, Science and Art Faculty of Gazi University Press, Ankara, 1983.

[39] Erişir, T., Yıldırım, E., *On the fundamental spinor matrices of real quaternions*, WSEAS Transactions on Mathematics, 22, 854-866, 2023.



Existence and Uniqueness of Almost Periodic Solutions to Time Delay Differential Equations

Münevver TUZ*

Firat University, Faculty of science, Department of Mathematics, 23100, Elazig, Turkey
mtuz@firat.edu.tr, ORCID: 0000-0002-9620-247X

Received: 10.10.2023

Accepted: 30.05.2024

Published: 30.06.2024

Abstract

In this study, a time-delayed relational neural network model was examined. The existence of almost periodic solutions of time delay differential equation has been investigated, and its uniqueness and stability have been proven with the help of Lyapunov point theorem and differential inequality. Since the signal transmission process of the neural network changes periodically in the real world, many scientists have focused on this issue and the almost periodic function has gained great importance because it is more suitable for practical events. The results found are different from and complementary to the previous ones.

Keywords: Almost Periodic; Lyapunov point theorem; Globally exponentially stable; Time-Varying Delays; Neural; Dynamic system.

Zaman Gecikmeli Diferansiyel Denklemlerin Yaklaşık Periyodik Çözümlerinin Varlığı ve Tekliği

Öz

Bu çalışmada zaman gecikmeli bir ilişkiyel sinir ağı modeli incelenmiştir. Zaman gecikmeli diferansiyel denklemin neredeyse periyodik çözümlerinin varlığı araştırılmış, Lyapunov nokta teoremi ve diferansiyel eşitsizlik yardımıyla tekliği ve kararlılığı kanıtlanmıştır. Gerçek dünyada sinir ağının sinyal iletim süreci periyodik olarak değiştiğinden, birçok bilim adamı bu konuya ağırlık vermiş ve



pratik olaylara daha uygun olması sebebi ile yaklaşık periyodik fonksiyon çok önem kazanmıştır. Bulunan sonuçlar öncekilerden farklı ve onları tamamlayıcı niteliktedir.

Anahtar Kelimeler: Yaklaşık periyodik; Lyapunov nokta teoremi; Küresel olarak kararlı; Zamanla Değişen Gecikmeler; Sinirsel; Dinamik sistem.

1. Introduction

Identifying and solving complex problems that cannot be solved with ordinary algorithms that we encounter in daily life is an interesting situation. Neural networks, which can both produce solutions to complex problems and are used in many multidisciplinary fields, have become a topic of current study and have attracted the attention of many writers, giving them the opportunity to be applied in different fields.

The first developed Hopfield artificial neural network model is considered to be the basis of neural networks. Hopfield proposed a Lyapunov function with positive values for this artificial neural network, which is a dynamic model [1]. This function is neural and is based on the presence of symmetric connection matrices in networks. Hopfield showed that the time derivative of this function is negative. This shows the stability of the system. The global stability of the system is proven by the symmetric connection matrix. Also, it is necessary to understand the properties of the activation functions and the values of the connection coefficients between neurons. Delay in the model is important for dynamic behavior. This delayed model was modeled using a circuit comprising neurons, an operational amplifier, and its connected resistance and capacitance elements. Dynamic neural network models have been frequently used in applications such as classification of examples, optimization and associative memory. Additionally, Cohen-Grossberg neural network models were examined and used to solve optimization problems, scientific fields and computational technology, and analog-digital converter design.

Cellular neural networks were discussed for the first time by L. O. Chua and L. Yang [2]. Cellular artificial neural networks consist of interconnected and mostly two-dimensional cells. The most important feature that distinguishes this structure from other models is that the connection weight coefficients create an invariant connection network on the studied plane. Cellular artificial neural networks have known features. In addition, because of their two-dimensional structure, they are frequently used in subjects such as image processing and pattern recognition. Relational memory networks are also important neural networks. Associative systems differ from those that can establish relationships between certain input and output vectors. Associative memory networks must remember the examples given to them during training, they memorize or store these examples. Associative memory networks are frequently used in applications such as pattern recognition, prediction, and completion of correct data from missing data.

For neural dynamic systems, the stability feature is a phenomenon that needs to be examined separately because it includes many dynamic behaviors. It affects some dynamic situations, such as the periodic oscillation behavior of the stability feature. The stability of delayed neural networks has many applications in many fields and has become an important argument in scientific studies. Application areas in the scientific field are image and signal processing, pattern recognition, optimization, etc. it is in the form. Time-varying delays in network activations are possible. The phenomenon of signal transmission in neural networks corresponds to periodic problems in applied sciences, and when there is a delay in the problems, stability analysis comes into play. To date, many researchers have addressed and examined the almost periodic problems we encounter in neural networks. In the neural network system, negative feedback can be called forgetting delay. Dependent population dynamics and neutral type time delays seen in vibrating bodies have recently become widely used. According to research, the number of papers on the stability and existence of an almost periodic solution in neutral neural networks with time-varying delays is small. Therefore, this study has an important place in the literature.

The existence of delayed almost periodic solutions for some energy-consuming systems in the generalized single-layer case in neural networks belongs to Kato [3]. Similarly, almost periodic solutions for nonlinear systems are given in [4,5]. There is also the theory of almost periodic functions for delayed differential equations and the first studies on the existence of ordinary or almost periodic solutions [6,7]. Li et al. [8] studied nearly periodic solutions and global exponential synchronization for delayed quaternion-valued neural networks. Researchers have recently produced interesting results on the stability of neural networks [9-12]. The almost periodic function, which is a continuation of the periodic function, was preferred by many scientists because it was more suitable for practical events and was introduced into mathematics by Bohr [13]. Stepanov processed periodicity without using continuity. Studies on the Bohr theory are given in general form in [14-19]. The results obtained have become one of the most special research topics in qualitative theory because of their importance and applications in physical science. The existence of almost periodic, asymptotically almost periodic and pseudo almost periodic solutions are among the most interesting topics of the qualitative theory of differential equations and difference equations, especially due to their applications in biology, economics and physics, and the researches have gained an important place in different fields [20-22].

In this study, the existence, stability and effects of an almost periodic solution for a time-delayed neural network model were investigated. Almost periodic solutions of a neutral bidirectional associative memory (BAM) neural network based on time-varying delays have been studied. In the light of the studies carried out, the delayed association neural network model was examined in this article. The existence and stability of nearly periodic solutions of the neutral BAM neural network based on varying delays were investigated. The existence of an almost periodic solution for this neural network was examined. Unlike other studies, behavioral solutions are examined directly in the field of memory. In the solutions of discontinuous neural networks, findings are created that will discover the chaos in the

neuron and create inertia and nonlinear effects. These results extend neural networks and some previously known networks to some extent under given conditions. Thus, the study complements previous results. We initially describe the sufficient conditions for existence and stability, along with some definitions and preliminary results. We will use these to prove our main results. In section 3, we demonstrate the uniqueness and stability of the almost-periodic solution of the neutral neural network determined by time-varying delays.

2. Materials and Methods

2.1 Preliminaries

In the first part, we will give basic information about the subject, its features and the methods used in the analysis. We aim to prove our main results using these. First, let's give the properties of the almost periodic solution of a neutral neural network. What we consider in this study

$$u_i'(t) = -a_i u_i(t) + \sum_{j=1}^n w_{ij} g_j(u_j(t)) + \sum_{j=1}^n v_{ij} g_j(u_j(t-\tau)) + \sum_{j=1}^n z_{ij} (u_j(t-\tau)) + \varphi_i, \quad (2.1)$$

here $u_i(t)$ is the state vector of the time t . The constants $a_i, w_{ij}, v_{ij}, z_{ij}$ are the connection weight parameters of the neural networks, φ_i is the output value, and $a_i, w_{ij}, v_{ij}, z_{ij}, \varphi_i: R \rightarrow R$ are almost periodic function for $i, j = 1, 2, \dots, n$, $\tau > 0$ correspond to leakage and transmission delay respectively, g_j is the activation function of the i th neurons and the initial conditions with the equation (2.1) are of the form,

$$u_i(k) = \delta_i(k) \text{ for all } k \in [-\infty, 0], \quad i = 1, 2, \dots, n,$$

where $\delta_i(\cdot)$ are continuous and real valued functions.

The aim of this study is to establish sufficient conditions for the existence and uniqueness of nearly periodic solutions for a given neural network. We can explain the theory of almost periodic functions as follows; for any $\epsilon > 0$, it is possible to find a real number $l = l(\epsilon) > 0$, for any interval with length $l(\epsilon)$, there exists a number $Y = Y(\epsilon)$ in this interval such that,

$$\begin{aligned} |a_i(t+Y) - a_i(t)| < \epsilon, & |w_{ij}(t+Y) - w_{ij}(t)| < \epsilon, & |v_{ij}(t+Y) - v_{ij}(t)| < \epsilon, \\ |\varphi_i(t+Y) - \varphi_i(t)| < \epsilon, & |z_{ij}(t+Y) - z_{ij}(t)| < \epsilon, & \text{for all } t \in R. \end{aligned}$$

Equilibrium Point: If the condition $f(x_e, t) = 0$ is satisfied for every $t \geq t_0$, then x_e is the equilibrium point of the system $\dot{x} = f(x, t)$, $x(t_0) = x_0$.

Theorem 2.1 (Lyapunov Stability Theorem) ([20]). Let the equilibrium point be $x = 0$ for a system given as $\dot{x} = f(x)$. Let $V(x): R^n \rightarrow R$ be a continuous and differentiable function. The time derivative of the function $V(x)$ is denoted by $\dot{V}(x)$ and is expressed as follows,

$$\dot{V}(x) = \sum_{i=1}^n \frac{\partial V(x)}{\partial x_i} \dot{x}_i = \sum_{i=1}^n \frac{\partial V(x)}{\partial x_i} f_i(x_i) = \sum_{i=1}^n \frac{\partial V(x)}{\partial x_i} f(x).$$

i) If $V(0) = 0, V(x) > 0, \forall x \neq 0$ and $\dot{V}(x) \leq 0, \forall x \in R^n$ if the condition is met, it is stable for $x = 0$.

ii) If the condition $\dot{V}(x) < 0, \forall x \neq 0$ is satisfied, $x = 0$ is asymptotically stable.

iii) If the condition $\dot{V}(x) > 0, \forall x \neq 0$ is satisfied, $x = 0$ is unstable.

It follows from this theorem that;

The function $\dot{V}(x)$ is negative semi-definite (i.e., $\dot{V}(x) \leq 0, \forall x \neq 0$), and $V(x)$ is a continuously differentiable positive definite function (i.e., $V(x) > 0, \forall x \neq 0$), the equilibrium point is stable.

If $\dot{V}(x)$ is strictly negative definite ($\dot{V}(x) < 0, \forall x \neq 0$), the equilibrium point is asymptotically stable.

If $\dot{V}(x)$ is positive definite ($\dot{V}(x) > 0, \forall x \neq 0$), the equilibrium point is unstable.

Lyapunov Stability Theorem is used to draw a conclusion about the stability properties of the equilibrium point and can characterize the stability of the equilibrium point by defining a positive energy function and examining its time derivative. One of the advantages of this theorem, called the Direct Method of Lyapunov Stability Theorem, allows us to determine the stability properties of the equilibrium point without solving the differential equation of the system.

Definition 2.2 ([6]). A continuous function $x : R \rightarrow R^n$ is said to be almost periodic on R if, for any $\epsilon > 0$, the set $T(u, \epsilon) = \{Y : \|u(t + Y) - u(t)\| < \epsilon \text{ for all } t \in R\}$ is relatively dense, for any $\epsilon > 0$, it is possible to find a real number $l = l(\epsilon) > 0$ with the property that, for any interval with length $l(\epsilon)$, there exists a number $Y = Y(\epsilon)$ in this interval such that

$$\|u(t + Y) - u(t)\| < \epsilon \text{ for all } t \in R.$$

Lemma 2.3 ([21]). Let $S^*(t) = (u_1^*(t), u_2^*(t), \dots, u_n^*(t))^T$ be an almost-periodic solution of equation (2.1) with initial value $(\phi_1^*(t), \phi_2^*(t), \dots, \phi_n^*(t))^T$. If there $\delta > 0$ and $K > 1$ such that for all solution $S(t) = (u_1(t), u_2(t), \dots, u_n(t))^T$ be the solution of equation (2.1) with initial value,

$$|u_i(t) - u_i^*(t)| \leq Ke^{-\delta t} \|\phi - \phi^*\|, t > 0, i = 1, 2, \dots, n, \text{ where}$$

$$\|\phi - \phi^*\| = \sup \max_{1 \leq j \leq n} |\phi_i(t) - \phi_i^*(t)|. \text{ Then } S^*(t) \text{ is said to be globally exponentially stable.}$$

In addition, we assume that the following conditions are met,

H1) $a_i > 0, w_{ij}, v_{ij}, z_{ij} : R \rightarrow R$ all continuous almost periodic functions, where a_i and $\tau > 0$ are constants and $i, j = 1, 2, \dots, n$.

H2) The constants $a_i, w_{ij}, v_{ij}, z_{ij}$ and ϕ_i are taken as follows:

$$\bar{a}_i = \sup_{t \in R} |a_i(t)|, \bar{w}_{ij} = \sup_{t \in R} |w_{ij}(t)|, \bar{v}_{ij} = \sup_{t \in R} |v_{ij}(t)|,$$

$$\bar{z}_{ij} = \sup_{t \in R} |z_{ij}(t)|, \bar{\phi}_i = \sup_{t \in R} |\phi_i(t)|, i, j = 1, 2, \dots, n.$$

H3) For each $j \in \{1, 2, \dots, n\}$, is with Lipschitz constant U_j ,

$$|g_j(u_j) - g_j(v_j)| \leq U_j |u_j - v_j|, \quad u_j, v_j \in R.$$

H4) There exist constants $\eta > 0$ and $i, j = 1, 2, \dots, n$, such that for all $t \in R$, there holds

$$-a_i(t) + \xi_i^{-1} \sum_{j=1}^n [|w_{ij}| + |v_{ij}| + |z_{ij}|] U_j, \quad \xi_j < -\eta < 0.$$

2.2. Existence of Almost Periodic Solutions

In this section, the existence and stability of the almost periodic solution of the equation (2.1) under the given conditions will be demonstrated.

Theorem 2.4. Assume that (H1)–(H4) are satisfied. In this case, the equation (2.1) has a unique, continuously differentiable, almost periodic solution.

Proof. Let's take $\bar{u}_i(t) = \xi_i^{-1} u_i(t)$.

Now we can convert (2.1) into the following equation,

$$\begin{aligned} \bar{u}'_i(t) &= -a_i \bar{u}_i(t) \\ &+ \xi_i^{-1} \sum_{j=1}^n w_{ij} g_j \xi_i(\bar{u}_j(t)) + \xi_i^{-1} \sum_{j=1}^n v_{ij} g_j \xi_i(\bar{u}_j(t - \tau)) + \xi_i^{-1} \sum_{j=1}^n z_{ij} \xi_i(\bar{u}_j(t - \tau)) + \xi_i^{-1} \varphi_i \end{aligned}$$

Let $\forall \theta \in B$ be a Banach space and then, B is a Banach space, we consider the almost periodic solution $u^\theta(t)$ of nonlinear almost periodic differential equations,

$$\begin{aligned} \bar{u}'_i(t) &= -a_i \bar{u}_i(t) \\ &+ \xi_i^{-1} \sum_{j=1}^n w_{ij} g_j \xi_i(\theta_j(t)) + \xi_i^{-1} \sum_{j=1}^n v_{ij} g_j \xi_i(\theta_j(t - \tau)) + \xi_i^{-1} \sum_{j=1}^n z_{ij} \xi_i(\theta_j(t - \tau)) + \xi_i^{-1} \varphi_i \end{aligned}$$

Let us obtain an almost periodic solution of equation (2.1),

$$\begin{aligned} u^\theta(t) &= (u_1^\theta(t), u_2^\theta(t), \dots, u_n^\theta(t))^T \\ &= (e^{\int_{-k}^t u_1(k) dk} \left[\xi_n^{-1} \sum_{j=1}^n w_{1j} g_j \xi_n(\theta_j(k)) + \xi_n^{-1} \sum_{j=1}^n v_{1j} g_j \xi_n(\theta_j(k - \tau)) + \right. \\ &\left. \xi_n^{-1} \sum_{j=1}^n z_{1j} \xi_n(\theta_j(k - \tau)) + \xi_n^{-1} \varphi_1(k) \right] dk, \dots, e^{\int_{-k}^t u_n(k) dk} \left[\xi_n^{-1} \sum_{j=1}^n w_{nj} g_j \xi_n(\theta_j(k)) + \right. \\ &\left. \xi_n^{-1} \sum_{j=1}^n v_{nj} g_j \xi_n(\theta_j(k - \tau)) + \xi_n^{-1} \sum_{j=1}^n z_{nj} \xi_n(\theta_j(k - \tau)) + \xi_n^{-1} \varphi_n(k) \right] dk)^T. \end{aligned} \tag{2.2}$$

Let's define the transformation $A : B \rightarrow B$ as follows:

$$A \theta(t) = u^\theta(t), \quad \forall \theta \in B.$$

We can prove that the transformation of A corresponds to the contraction of B . We will prove that there is a mapping. Using Lemma (2.3), (H1-H4), for $\forall \theta, \psi \in B$,

$$|A(\theta(t)) - A(\psi(t))| = (|A(\theta(t)) - A(\psi(t))|_1, \dots, |A(\theta(t)) - A(\psi(t))|_n)^T$$

$$\begin{aligned}
 &= \left(\left| e^{\int_{-k}^t u_1(k) dk} \left[\xi_n^{-1} \sum_{j=1}^n w_{1j} (g_j \xi_n (\theta_j(k)) - (g_j \xi_n (\psi_j(k))) + \xi_n^{-1} \sum_{j=1}^n v_{1j} (g_j \xi_n (\theta_j(k - \tau)) - \right. \right. \right. \\
 & \left. \left. \left. g_j \xi_n (\psi_j(k - \tau)) \right) + \xi_n^{-1} \sum_{j=1}^n z_{1j} (\xi_n (\theta_j(k - \tau)) - \xi_n (\psi_j(k - \tau))) \right] dk \right|, \dots, \\
 & \left| e^{\int_{-k}^t u_n(k) dk} \left[\xi_n^{-1} \sum_{j=1}^n w_{nj} (g_j \xi_n (\theta_j(k)) - g_j \xi_n (\psi_j(k))) + \xi_n^{-1} \sum_{j=1}^n v_{nj} (g_j \xi_n (\theta_j(k - \tau)) - \right. \right. \\
 & \left. \left. \left. g_j \xi_n (\psi_j(k - \tau)) \right) + \xi_n^{-1} \sum_{j=1}^n z_{nj} (\xi_n (\theta_j(k - \tau)) - \xi_n (\psi_j(k - \tau))) \right] dk \right|^T \\
 &\leq (e^{\int_{-k}^t u_1(k) dk} \left[\sum_{j=1}^n \overline{w_{1j}} U_j \left| (\theta_j(k)) - (\psi_j(k)) \right| + \sum_{j=1}^n \overline{v_{1j}} U_j \left| (\theta_j(k - \tau)) - (\psi_j(k - \tau)) \right| + \right. \\
 & \left. \sum_{j=1}^n \overline{z_{1j}} U_j \left| (\theta_j(k - \tau)) - (\psi_j(k - \tau)) \right| \right] dk, \dots, e^{\int_{-k}^t u_n(k) dk} \left[\sum_{j=1}^n \overline{w_{nj}} U_j \left| (\theta_j(k)) - (\psi_j(k)) \right| + \right. \\
 & \left. \xi_n^{-1} \sum_{j=1}^n \overline{v_{nj}} U_j \left| (\theta_j(k - \tau)) - (\psi_j(k - \tau)) \right| + \sum_{j=1}^n \overline{z_{nj}} U_j \left| (\theta_j(k - \tau)) - (\psi_j(k - \tau)) \right| \right] dk)^T \\
 &\leq \sum_{j=1}^n \overline{w_{1j} + v_{1j}} + \overline{z_{1j}} U_j \sup \left| (\theta_j(k)) - (\psi_j(k)) \right|, \dots, \sum_{j=1}^n \overline{w_{nj} + v_{nj}} + \overline{z_{nj}} U_j \sup \left| (\theta_j(k)) \right. \\
 & \quad \left. - (\psi_j(k)) \right|^T \\
 &= (\sup \left| (\theta_j(k)) - (\psi_j(k)) \right|, \dots, \sup \left| (\theta_j(k)) - (\psi_j(k)) \right|)^T \tag{2.3}
 \end{aligned}$$

Let m be a positive integer. Then, from (2.3), we get

$$\begin{aligned}
 &= (\sup \left| A^m (\theta_j(k)) - A^m (\psi_j(k)) \right|_1, \dots, \sup \left| A^m (\theta_j(k)) - A^m (\psi_j(k)) \right|_n)^T \\
 &= (\sup \left| A(A^{m-1} (\theta_j(k)) - A^{m-1} (\psi_j(k))) \right|_1, \dots, \sup \left| A(A^{m-1} (\theta_j(k)) - A^{m-1} (\psi_j(k))) \right|_n)^T \\
 &\leq (\sup \left| (\theta_j(k)) - (\psi_j(k)) \right|_1, \dots, \sup \left| (\theta_j(k)) - (\psi_j(k)) \right|_n)^T \\
 &= (\sup \left| (\theta_j(k)) - (\psi_j(k)) \right|, \dots, \sup \left| (\theta_j(k)) - (\psi_j(k)) \right|)^T \tag{2.4}
 \end{aligned}$$

In view of (3.3) we have

$$\begin{aligned}
 &\left| A^N ((\theta(t))) - A^N (\psi(t)) \right|_i \leq \sup \left| A^N (\theta(t)) - A^N (\psi(t)) \right|_1 \leq \\
 &\sum_{j=1}^n l \sup \left| ((\theta(t))) - (\psi(t)) \right| \leq \sup \max_{1 \leq j \leq n} \left| ((\theta(t))) - (\psi(t)) \right| \sum_{j=1}^n l \leq \|(\theta(t)) - (\psi(t))\|
 \end{aligned}$$

for all $t \in R, i, j = 1, 2, \dots, n$. It follows that

$$\left\| (A^N (\theta(t))) - A^N (\psi(t)) \right\| = \sup \max_{1 \leq j \leq n} \left| (A^N (\theta(t))) - A^N (\psi(t)) \right| \leq \|(\theta(t)) - (\psi(t))\| \tag{2.5}$$

Thus, the condition given in Lemma (2.3) is met. This guarantees the existence and uniqueness of the almost periodic solution of equation (2.1) expressed in Theorem (2.4) and the proof is completed.

2.3. Globally Exponentially Stability of the Almost Periodic Solution

Theorem 2.5. Assume that (H1)–(H4) are satisfied. Then equation (2.1) has exactly one almost periodic solution $x^*(t)$. Moreover, this solution is globally exponentially stable.

Proof. Let $u^\theta(t) = (u_1^\theta(t), u_2^\theta(t), \dots, u_n^\theta(t))^T$ be a solution of equation (2.1) with initial conditions

$$u_i(k) = \delta_i(k), \quad |\delta_i(k)| < \rho, \quad k \in [-\infty, 0]. \quad i = 1, 2, \dots, n,$$

Thus, according to Lemma (2.3), the solution $u_i(k)$ is bounded and $|u_i(t)| < \rho$,

for all $t \in R, i = 1, 2, \dots, n$.

$S^*(t) = (x_1^*(t), x_2^*(t), \dots, x_m^*(t))^T$ be an almost-periodic solution of equation (2.1) with initial value $(\phi_1^*(t), \phi_2^*(t), \dots, \phi_n^*(t))^T$. If there $\delta > 0$ and $K > 1$ such that for all solution $S(t) = (x_1(t), x_2(t), \dots, x_n(t))^T$ be the solution of equation (2.1) with initial value, $\phi(t) = (\phi_1(t), \phi_2(t), \dots, \phi_n(t))^T$.

$y_j(t) = x_j(t) - x_j^*(t) = S(t) - S^*(t)$. Then

$$y_i'(t) = -a_i y_i(t) + \sum_{j=1}^n w_{ij} g_j(y_j(t)) + \sum_{j=1}^n v_{ij} g_j(u_j(t - \tau)) - (x_j(t - \tau)) + g_j(x_j^*(t - \tau)) + \sum_{j=1}^n z_{ij} (y_j(t - \tau)) + (x_j(t - \tau)) - z_{ij} (x_j^*(t - \tau)),$$

where $i = 1, 2, \dots, n$.

$$Y_i(t) = y_i(t)e^{it}, \quad i = 1, 2, \dots, n.$$

Then

$$\begin{aligned} D^- |x_i(t) - x_i^*(t)| &\leq -a_i |x_i(t) - x_i^*(t)| + \sum_{j=1}^n |w_{ij}| |g_j(x_j(t) - x_j^*(t))| \\ &\quad + \sum_{j=1}^n |v_{ij}| |g_j(u_j(t - \tau)) - (x_j(t - \tau)) + g_j(x_j^*(t - \tau))| \\ &\quad + \sum_{j=1}^n |z_{ij}| |(y_j(t - \tau)) + (x_j(t - \tau)) - z_{ij} (x_j^*(t - \tau))| \\ &\leq -a_i |x_i(t) - x_i^*(t)| + \sum_{j=1}^n (a_{ij}^+ + \alpha_{ij}^+ + \beta_{ij}^+) \times p_j |(x_j(t - \tau)) - (x_j^*(t - \tau))| \end{aligned} \tag{2.6}$$

where D^- denotes the upper left derivative. If we let $y_i(t) = x_i(t) - x_i^*(t)$ then

$$\begin{aligned} D^- |y_i(t)| &\leq -a_i y_i(t) + \sum_{j=1}^n (a_{ij}^+ + \alpha_{ij}^+ + \beta_{ij}^+) \sup |y_j(s)| \\ &= -a_i y_i(t) + \sum_{j=1}^n (a_{ij}^+ + \alpha_{ij}^+ + \beta_{ij}^+) p_j \bar{y}_j(t), \end{aligned} \tag{2.7}$$

where $\bar{y}_j(t) = \sup |y_j(s)|$. From Lemma (2.3) we can see that a vector exists.

$\eta = (\eta_1, \eta_2, \dots, \eta_n)^T$ such that

$$= -a_i y_i(t) + \sum_{j=1}^n (a_{ij}^+ + \alpha_{ij}^+ + \beta_{ij}^+) p_j \eta_j < 0,$$

We can choose a small positive constant $\delta < 1$ such that, for $i = 1, 2, \dots, n$.

$$\delta \eta_i + \left[-a_i y_i(t) + \sum_{j=1}^n (a_{ij}^+ + \alpha_{ij}^+ + \beta_{ij}^+) p_j \eta_j e^{-\delta t} \right] < 0.$$

For constant value $\gamma > 1$,

$$\gamma \eta_i e^{-\delta t} > 1, \quad \forall t \in [-\tau, 0]. \text{ For } \varepsilon > 0,$$

$$Y_i(t) = \gamma \eta_i \left[\sum_{j=1}^n \bar{y}_j(0) + \varepsilon \right] e^{-\delta t}, i = 1, 2, \dots, n. \tag{2.8}$$

From (2.7) and (2.8)

$$\begin{aligned} D_- Y_i(t) &= -\delta \gamma \eta_i \left[\sum_{j=1}^n \bar{y}_j(0) + \varepsilon \right] e^{-\delta t} \\ &> \left[-a_i \eta_i + \sum_{j=1}^n (a_{ij}^+ + \alpha_{ij}^+ + \beta_{ij}^+) p_j \eta_j e^{-\delta t} \right] \gamma \times \left[\sum_{j=1}^n \bar{y}_j(0) + \varepsilon \right] e^{-\delta t} \\ &= -a_i \eta_i \gamma \left[\sum_{j=1}^n \bar{y}_j(0) + \varepsilon \right] e^{-\delta t} + \sum_{j=1}^n (a_{ij}^+ + \alpha_{ij}^+ + \beta_{ij}^+) p_j \eta_j \gamma \\ &\quad \times \left(\sum_{j=1}^n \bar{y}_j(0) + \varepsilon \right) e^{-\delta(t-\tau)}, \\ Y_i(t) &= \gamma \eta_i \left[\sum_{j=1}^n \bar{y}_j(0) + \varepsilon \right] e^{-\delta t} > \sum_{j=1}^n \bar{y}_j(0) + \varepsilon > |y_i(t)|. \end{aligned} \tag{2.9}$$

Here

$$|y_i(t_i)| < Y_i(t_i), \text{ for } i = 1, 2, \dots, n \text{ and } t_i > 0,$$

$$|y_i(t_i)| - Y_i(t_i) = 0,$$

We get

$$0 \leq D^- |y_i(t_i) - Y_i(t_i)| = D^- |y_i(t_i)| - D_- Y_i(t_i)$$

and

$$D^- |y_i(t_i)| \leq D_- Y_i(t_i).$$

Let $\varepsilon \rightarrow 0$ and $K = \max_{1 \leq j \leq n} \{\eta_j \gamma + 1\}$. Then

$$|x_i(t) - x_i^*(t)| = |y_i(t)| \leq \eta_i \gamma \sum_{j=1}^n \bar{y}_j(0) e^{-\delta t} \leq \eta_i \gamma e^{-\delta t} \|\phi - \phi^*\| \leq K e^{-\delta t} \|\phi - \phi^*\|.$$

From the assumption Lemma (2.3), the solution $x^*(t)$ is globally exponentially stable.

3. Results and Discussion

The existence of almost periodic functions is especially important in applications such as time series analysis or waveform processing. At the same time, the global stability of artificial neural networks is also critical. The training process of the network occurs by optimizing the weights, which usually starts randomly at the beginning. Global stability means that this optimization can achieve similar results even if started from different starting points. This ensures that the learning process of the network is more reliable and repeatable.

Especially for the analysis of almost periodic functions, it is important that the network can consistently recognize and learn patterns over time. The existence and uniqueness of periodic solutions provide important information for understanding and analyzing the behavior of a system or equation. With stability analysis, the existence of almost periodic solutions can help evaluate the stability of equilibrium states or solutions in a system. Especially in mathematical modeling, these solutions are used to predict the behavior of the system. Almost periodic solutions can represent changes and cyclical behavior of a system over time. This is important for understanding and predicting system dynamics,

especially for understanding the complexity of systems in fields such as engineering, physics, biology. Periodic solutions can form the basis for frequency analysis, especially in signal processing and control systems. It is used to understand, design and optimize the frequency response of systems. By measuring stability and reliability, almost uniqueness of periodic solutions means that a system behaves in a unique way under certain conditions. This is important to evaluate the stability of the system and predict how it will react to certain inputs or conditions. For these reasons, the existence and uniqueness of almost periodic solutions provide a powerful analysis tool for understanding and managing the complexity of systems in science, engineering and mathematics.

4. Conclusion

Artificial neural networks consist of interconnected and mostly two-dimensional cells. The most important feature that distinguishes this structure from other models is that the connection weight coefficients create an invariant connection network in the studied plane. Due to the limited speed of neurons, chaos, oscillation, instability, etc. may occur in the signal transmission between neurons. It occurs when the system is stable and manifests itself in some dynamics that will affect the stability of the system, but it also includes many dynamic behaviors such as periodic oscillatory behavior that is almost periodic. In artificial neural networks, not all cells are connected to each other, but are directly connected only to their neighbors, which reduces the complexity of the network structure and reduces energy consumption. Relational memory networks, one of the most important classes of artificial neural networks, are frequently used in applications such as pattern recognition, predicting and completing correct data from missing data. It also includes many dynamic behaviors such as periodic oscillatory behavior, almost periodic neural network models are widely used in solving optimization problems, in scientific fields and computing technology, in various engineering fields such as analog to digital converter design. It is very important to determine the stability of artificial neural networks designed in applications. The artificial neural network created in the type of neural network examined must have a single stable balance point. Repeating complex situations are represented by periodicity, and the dynamics and biological mechanisms of time-delayed periodic systems are discussed under the name of neural network construction. Many researchers who have addressed the near-periodic problems of neural networks have called the negative feedback state of the network system the forgetting delay. Dependent population dynamics and neutral type time delays occurring in vibrating masses have been widely used. However, there are very few papers focusing on the stability and existence of a nearly periodic solution for neutral neural networks with time-varying delays in terms of leakage. For this reason, the existence and stability of solutions to almost periodic problems is an issue that needs to be emphasized. Recently, some researchers have attached great importance to the one-way neutral type. Hopfield's dual associative memory model is of great importance for pattern recognition and automatic control applications. In this study, the existence and stability of the nearly periodic solution has been proven and its effects have

been investigated. Near-periodic solutions of the neutral neural network based on time-varying delays have been studied. Although the results obtained cannot be directly applied to many arrangements, they do extend some known networks to some extent. The contribution of this article to science is in the solutions of discontinuous neural networks, findings that will reveal the chaos in the neuron and create inertia and nonlinear effects. Therefore, it is important that the results complement previous studies.

Acknowledgements

Not applicable.

References

- [1] Hopfield, J.J., *Neuron with graded response have collective computational properties like those of two-state neurons*, Proceedings of the National Academy of Sciences of the United States of America, 81, 3088–92, 1984.
- [2] Chua, L. O., Yang, L., *Cellular Neural Networks Theory*, IEEE Transactions Circuits and Systems, 35, 10, 1257-1272, 1988.
- [3] Kato, S., Imai, M., *On the existence of periodic and almost periodic solutions for nonlinear systems*, Nonlinear Analysis, TMA 24, 1183-1192, 1995.
- [4] Kartsatos, A.G., *Almost periodic solutions to nonlinear systems*, Bollettino dell'Unione Matematica Italiana, 9, 10-15, 1974.
- [5] Seifert, G., *Almost periodic solutions for a certain class of almost periodic systems*, Proceedings of the American Mathematical Society, 84, 47-51, 1982.
- [6] Levitan, B.M., Zhikov, V.V., *Almost Periodic Functions and Differential Equations*, Cambridge University. Press, Cambridge, 1982.
- [7] Hall, J.K., *Periodic and almost periodic solutions of functional-differential equations*, Archive for Rational Mechanics and Analysis, 15, 289-304, 1964.
- [8] Li, Y.K., Lv, G., Meng, X.F., *Weighted pseudo-almost periodic solutions and global exponential synchronization for delayed QVCNNs*, Journal of Inequalities and Applications, 1, 1–23, 2019.
- [9] Tian, Y.F., Wang, Z.S., *Stochastic stability of Markovian neural networks with generally hybrid transition rates*, IEEE Transactions on Neural Networks and Learning Systems, <https://doi.org/10.1109/TNNLS.2021.3084925>
- [10] Hou, Y.Y., Dai, L.H., *Square-mean pseudo almost periodic solutions for quaternion-valued stochastic neural networks with time-varying delays*, Mathematical Problems in Engineering 2021, 6679326, 2021.
- [11] Li, Y.K., Meng, X.F., *Almost automorphic solutions in distribution sense of quaternion-valued stochastic recurrent neural networks with mixed time-varying delays*, Neural Processing Letters, 51(4), 1353–1377, 2020.
- [12] Yang, T.Q., Xiong, Z.L., Yang, C.P., *Analysis of exponential stability for neutral stochastic Cohen–Grossberg neural networks with mixed delays*, Discrete Dynamics in Nature and Society 2019, 4813103, 2019.
- [13] Bohr, H., *Zur Theorie der fast periodischen Funktionen I*, Acta Mathematica, 45, 29–127, 1925.
- [14] Andres, J., Pennequin, D., *On Stepanov almost-periodic oscillations and their discretizations*, Journal of Difference Equations and Applications, 18(10), 1665–1682, 2012.

- [15] Andres, J., Pennequin, D., *On the nonexistence of purely Stepanov almost-periodic solutions of ordinary differential equations*, Proceedings of the American Mathematical Society, 140(8), 2825–2834, 2012.
- [16] Maqbul, Md., Bahuguna, D., *Almost periodic solutions for Stepanov-almost periodic differential equations*, Differential Equations and Dynamical Systems, 22, 251–264, 2014.
- [17] Henríquez, H.R., *On Stepanov-almost periodic semigroups and cosine functions of operators*, Journal of Mathematical Analysis and Applications, 146(2), 420–433, 1990.
- [18] Jiang, Q.D., Wang, Q.R., *Almost periodic solutions for quaternion-valued neural networks with mixed delays on time scales*, Neurocomputing, 439, 363–373, 2021.
- [19] Wang, T.Y., Zhu, Q.X., Cai, W., *Mean-square exponential input-to-state stability of stochastic fuzzy recurrent neural networks with multi-proportional delays and distributed delays*, Mathematical Problems in Engineering 2018, 6289019, 2018.
- [20] Doğan, Z., *The investigation of stability properties of neutral type time delayed dynamic neural networks*, Istanbul University-Cerrahpasa Institute of Graduate Studies Department of Computer Engineering, M.Sc. Thesis, 2019.
- [21] Xu, C., Mao, X., *Existence and Exponential Stability of Anti-periodic Solutions for A Cellular Neural Networks with Impulsive Effects*, Wseas Transactions on Signal Processing, 11, 140-149, 2015.
- [22] Wang, P., Li, B., Li, Y.K., *Square-mean almost periodic solutions for impulsive stochastic shunting inhibitory cellular neural networks with delays*, Neurocomputing, 167, 76–82, 2015.



Structural and Luminescence Characterization of LiAlO₂ Ceramics Synthesized by Sol-Gel Technique

Volkan ALTUNAL^{1,*}

¹*Cukurova University, Art Sciences Faculty, Department of Physics, 01250 Adana, TÜRKİYE*
valtunal@cu.edu.tr, ORCID: 0000-0001-9411-3441

Received: 24.05.2024

Accepted: 23.06.2024

Published: 28.06.2024

Abstract

This study aims to produce lithium aluminate (LiAlO₂) materials as dense ceramics by the sol-gel method and to examine their structural and luminescence properties for radiation dosimetry applications. The crystal structures of ceramics synthesized using the XRD method were confirmed and their morphological properties were examined using SEM analysis. The defect concentrations and lattice parameters of LiAlO₂ were also discussed in depth. It has been found that LiAlO₂ ceramics have a total of three exponential decay function components that decay OSL signals fast, medium and slow. The TL glow curve of the material exhibited two TL peaks located around 110 and 200 °C. An intense luminescence band around 700 nm was found in RL and TL emissions, which is attributed to oxygen vacancies in the structure. Obtaining promising luminescence signals for passive dosimetry from LiAlO₂ samples in this study may make them a candidate dosimeter for radiation dosimetry applications with further studies to be conducted in the future.

Keywords: LiAlO₂; Sol-Gel synthesis; Thermoluminescence; Optically stimulated luminescence; Radioluminescence.

* Corresponding Author

DOI: 10.37094/adyujsci.1489596.



Sol-Jel Tekniđi ile Sentezlenen LiAlO₂ Seramiklerinin Yapısal ve Lüminesans Karakterizasyonu

Öz

Bu çalışma, lityum alüminat (LiAlO₂) malzemelerinin sol-jel yöntemiyle yoğun seramikler halinde üretilmesini ve radyasyon dozimetri uygulamaları için yapısal ve lüminesans özelliklerinin incelenmesini amaçlamaktadır. XRD yöntemi kullanılarak, sentezlenen seramiklerin kristal yapıları doğrulandı ve malzemenin morfolojik özellikleri SEM analizi kullanılarak incelendi. LiAlO₂'nin kusur konsantrasyonları ve kafes parametreleri de derinlemesine tartışıldı. LiAlO₂ seramiklerinin OSL sinyalleri hızlı, orta ve yavaş bozulum sergileyen toplam üç üstel bozunma fonksiyonu bileşenlerine sahip olduğu bulunmuştur. Malzemenin TL ışınma eğrisi, 110 ve 200 °C civarında bulunan iki TL tepe noktası sergiledi. RL ve TL emisyonlarında yapıdaki oksijen boşluklarına atfedilen 700 nm civarında yoğun bir lüminesans bandı bulundu. Bu çalışmada LiAlO₂ örneklerinden pasif dozimetri için umut verici lüminesans sinyallerinin elde edilmesi, gelecekte yapılacak başka çalışmalarla onları radyasyon dozimetri uygulamaları için aday bir dozimetre haline getirebilir.

Anahtar Kelimeler: LiAlO₂; Sol-Jel sentezi; Termolüminesans; Optik uyarımlı lüminesans; Radyolüminesans.

1. Introduction

Thermoluminescence (TL) and Optical Stimulated Luminescence (OSL) are known as passive dosimetry methods and are based on luminescence emission following thermal or optical excitation of previously irradiated insulator or semiconductor materials, respectively [1]. Although the OSL method, which is a newer method compared to TL, offers great convenience in application, the number of OSL dosimetry systems is insufficient due to the newness of the technology [2, 3]. This situation has recently led researchers to develop new OSL dosimeters, and many alternative host materials have been proposed in the literature [4-9]. Carbon-doped alumina (Al₂O₃:C) is well known in personal dosimetry for its superior properties for medical physics applications [10]. It remains the material of choice despite its non-tissue equivalence to Al₂O₃:C (Z_{eff} ~11.3), and non-sensitive to neutrons [11]. The way to develop a new OSL dosimeter could be a tissue-equivalent lattice. Moreover, certain critical properties are desirable in the development of materials with luminescent properties for OSL dosimetric applications. These include high radiation sensitivity, photosensitive trapped charges, linear behaviour in the dose-response relationship, minimal signal fading and resistance to external physical effects (e.g. mechanical stress and humidity). These properties are necessary to ensure that the material functions as an effective dosimeter.

Alkali aluminates are a lattice containing the elements alkali metals and aluminium, holding these two elements together with two oxygen atoms. The crystal structure of alkali aluminates can affect the placement of activator ions and the transitions between energy levels. Therefore, examining the luminescence properties of alkali aluminates is very important for optical and electronic applications [12-14]. Recently, their promising properties for LED applications, luminescence and imaging devices have been reported [15, 16]. In particular, LiAlO_2 is an important material for luminescence studies and dosimetric applications. LiAlO_2 is also known to have high thermal stability and dosimetric properties that can be used to detect ionization radiation [12, 17, 18]. Therefore, the luminescence development and characterization of LiAlO_2 may offer an infrastructure for important applications for dose measurement and radiation detection in fields such as medical imaging, radiotherapy, and nuclear medicine [19, 20]. Additionally, LiAlO_2 with an effective atomic number of 10.7, making it the superior dosimetric material over $\text{Al}_2\text{O}_3:\text{C}$ [21].

Although the luminescence sensitivity of pure LiAlO_2 has been reported to be low in the literature, the source of luminescence has not been fully identified, creating difficulties in optimizing and improving dosimetric properties. Therefore, in this study, LiAlO_2 ceramics were developed by the sol-gel method and their luminescence nature was examined in depth with RL, TL and OSL techniques.

2. Materials and Methods

2.1. Sample preparation

Figure 1 shows a simple schematic representation of the sol-gel pathway for LiAlO_2 ceramic pellets. The sol-gel route begins by dissolving nitrate-based Li and aluminium salts (purchased from Sigma Aldrich) in pure water in suitable molar ratios. After stirring for approximately 1 h at RT, citric acid (1:4, molar, purchased from Sigma Aldrich) was added to this mixture and the temperature was slowly increased to 80 °C. The dehydration process continued for approximately 24 hours. At the end of 24 hours, dried xerogel was achieved. 2-hour calcination treatment was applied at 900 °C to remove the organics that appeared in the structure during the formation of the crystal structure. As a result of the calcination route, pure LiAlO_2 white powders were obtained. LiAlO_2 powders were converted into 30 mg pellets using evacuable pellet dies in a manual pressing system before the sintering process. The dimensions of the prepared pellets were ~5.8 mm in diameter and ~0.70 mm in thickness. It should be noted that with the sintering treatment at 1300 °C for 4 hours, the mass of the ceramic pellets was measured to be approximately 24 - 24.8 mg. The final products were obtained as pellets with ~5.4 mm diameter and a ~0.5 mm thickness.

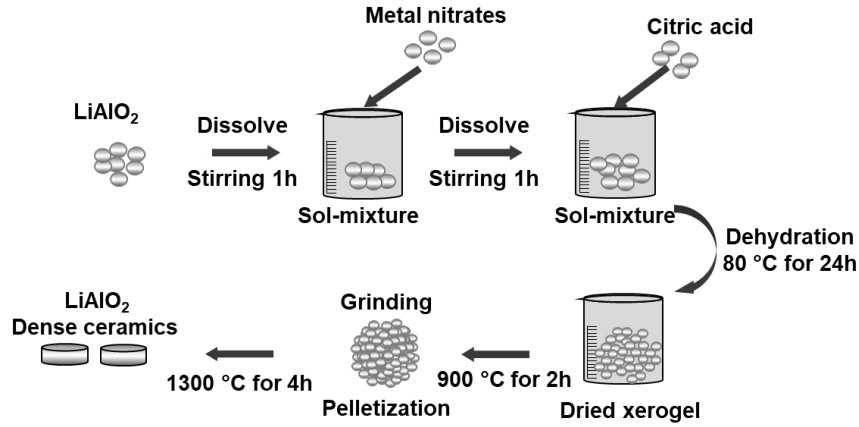


Figure 1: Schematic representation of the sol-gel process for LiAlO₂ ceramics

2.2. Characterization

To examine the structure and phase composition of LiAlO₂ crystals, X-ray diffraction (XRD) patterns were examined. The Panalytical Empyrean brand XRD analysis system used is equipped with a Cu-K α tube, $\lambda = 0.1541$ nm. Patterns were investigated by scanning 0.02° with a 2 θ scanning range from 10° to 90°. XRD ref. data from the International Center for Diffraction Data (ICDD) was used to identify crystalline phases.

The crystallite sizes of LiAlO₂ crystals were evaluated by the Debye-Scherrer formula [22];

$$D_{hkl} = K\lambda / (\beta_{hkl} \cos\theta) \quad (1)$$

Here D refers to the crystallite size (nm); hkl are Miller indices; K is a numerical factor set at 0.9; λ represents wavelength; θ is half of the diffraction angle; and β is the full width at half maximum (FWHM), measured in radians.

Besides crystallite size, strain (ϵ) values were also calculated using the following equation [23]:

$$\epsilon = \beta \cos\theta / 4 \quad (2)$$

where β is FWHM and θ represents half of the diffraction angle.

Another factor is the dislocation density (δ), which affects many properties of materials [24]. This density was determined by a special equation in LiAlO₂ crystals.:

$$\delta = 1/D^2 \quad (3)$$

where D represents the crystallite size of the LiAlO₂ crystals.

To examine the surface morphologies of LiAlO₂ ceramics, scanning electron microscope (SEM) photographs were taken using the Zeiss brand Supra 55 model SEM device. SEM photographs with

20000x direct magnification were obtained using 20 kV high voltage, and the grain size analysis of the surfaces was processed in the imageJ program.

2.3. Luminescence measurements

Luminescence signals of LiAlO₂ pellets were achieved using the DA-20 model Risø TL/OSL reader system of Danish origin. The system has a ⁹⁰Sr-⁹⁰Y radiation source (β) with 0.11 Gy/s. TL and OSL signals are captured with a EMI 9235QA PM tube. Hoya U-340 (100-400 nm permeability) filter was used in front of this PM tube. The OSL signals were acquired with 470 nm blue LED excitation. Prior to OSL readings, a preheating procedure was applied at 100 °C for 10 s to eliminate signals from unstable shallow traps. At the end of the OSL measurements, the samples were cleaned of residual doses by heating the samples to 450 °C with a heating rate of 5 °C/s. TL analyses were performed by heating the samples to 450 °C after irradiation with 2 °C/s, and background subtraction was necessarily applied. Background TL signals represent sample readings performed under the same conditions immediately after the initial TL reading.

Here, the analysis of OSL decay curves is based on a method based on fitting a combination of time decaying functions [25, 26]. The experimental OSL decay curve was analyzed by the first-order curve fitting. The fitting equation used for this analysis and representing the first-order kinetic approach can be written as following equation:

$$y = \text{background} + 1^{\text{st}} \text{ component} + 2^{\text{nd}} \text{ component} + 3^{\text{rd}} \text{ component} + \dots$$

$$I(t) = \text{background} + I_1 \exp\left(-\frac{t}{\tau_1}\right) + I_2 \exp\left(-\frac{t}{\tau_2}\right) + I_3 \exp\left(-\frac{t}{\tau_3}\right) + \dots \quad (4)$$

where 1st, 2nd, and 3rd components refer to the first-order components of OSL signals that decrease with time, respectively. While t is the duration of stimulation; $I(t)$ is the OSL signal intensity as a function of time. $I_{1,2,3}$ and $\tau_{1,2,3}$ represent the maximum intensities and lifetimes, respectively. Deconvolution quality was evaluated by calculating Figure of Merit (FOM) values for the experimental curve [27].

Radioluminescence (RL) emission spectra were acquired in a homemade RL system consisting of a miniature X-ray source, a QE Pro-model Ocean Optics spectrometer, an X-ray control unit, and a closed chamber. While the samples were exposed to approximately ~20 kV X-rays, emissions in the range of 200 nm to 1000 nm were observed from the sample. TL emission measurements, performed in the range from 50 °C to 400 °C at a heating rate of 2 °C/s, were performed on a similar homemade TL spectrometer following a 600 s x-ray irradiation. This system consists of a monochromator, a sample holder with a linear heater, and a CCD camera mounted on the monochromator window (ANDOR). Despite the wide spectral coverage range of CCD cameras, TL emissions have been obtained in the

range of 400 nm to 1000 nm, as their quantum efficiency decreases significantly in the ultraviolet (UV) region, especially below 400 nm.

3. Results and Discussion

3.1. Structural and Morphological Properties

The phase formations of LiAlO_2 powders were confirmed through XRD analysis and are shown in Fig. 2. As seen from the figure, the XRD patterns matched well with the XRD peaks of the LiAlO_2 tetragonal (phase characterized by the P 41 21 2 space group) reference ICDD 98-003-0249 PDF card. The absence of any peak originating from any secondary phase confirms the LiAlO_2 phase, indicates that LiAlO_2 ceramics have been successfully synthesized.

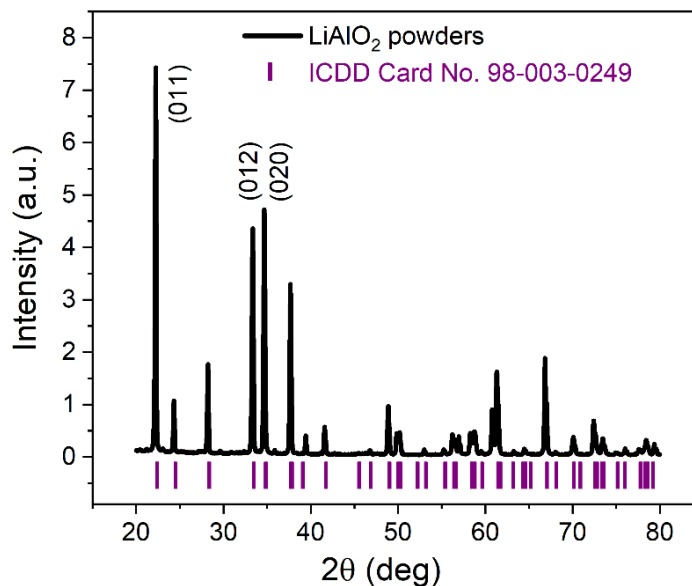


Figure 2: XRD pattern of the 1300 °C sintered LiAlO_2 powders prepared via sol-gel method

In Table 1, the Bragg angles represented with the three most intense diffraction peaks and the (011), (012), and (020), (hkl) planes are presented along with the structural parameters for the LiAlO_2 samples. The Eqn.1 was used to determine the crystallite size of each plane and the average crystallite size was calculated as 58.6 nm. In addition to the crystallite size, strain values were determined using the Eqn.2 for the (011), (012), and (020) planes and were found as 3.20×10^{-2} , 3.74×10^{-2} , and 3.74×10^{-2} , respectively. Another important parameter is the dislocation density (δ) values, which were found as 0.59×10^{20} , 0.41×10^{20} , and 0.41×10^{20} with the Eqn.3. As a result of phase analyses, it can be said that the crystallinity of LiAlO_2 powders are in compliance with the reference values and have good crystallinity.

Table 1. Positions of the diffraction peaks and structural parameters of LiAlO₂ powders

	hkl Planes		
	(011)	(012)	(020)
Peak Positions, 2θ , (°)	22.22	33.33	34.64
FWHM, β (°)	0.14	0.15	0.15
Crystalite size, D (nm)	64.92	55.51	55.42
Micro strain, $\varepsilon \times 10^{-2}$	3.19	3.74	3.74
Dislocation density, δ (10^{20})	0.51	0.44	0.44

Figure 3 shows SEM photographs and particle size distribution histogram bars curves of LiAlO₂ powder and pellet samples. Here, after the calcination process of the powder samples, they were sintered at 1300 °C without pelletizing. As seen in Fig. 3, the pellet surfaces presented a more homogeneous structure than the morphology in the photographs obtained from powder samples. Relatively more irregularly, large and small structures were observed in the powder samples, and an increase in the distribution of the structures forming local necks was observed with the sintering treatment. On the other hand, as the particles of the pellet samples were fused together by pressure, relatively non-porous, smooth and interconnected smaller particle size clusters were observed on their surfaces with high temperature sintering.

The size distribution of the particles in the samples was determined by measuring them in the ImageJ program from SEM images that fit the well-known size histogram with the log-normal function. It should be noted that at least 200 particle sizes were measured during the evaluation. The obtained histograms and log-normal functions and the mean particle size (D) and standard deviation (σ_D) values of each sample are presented together with the SEM images of the corresponding samples in Fig. 3.

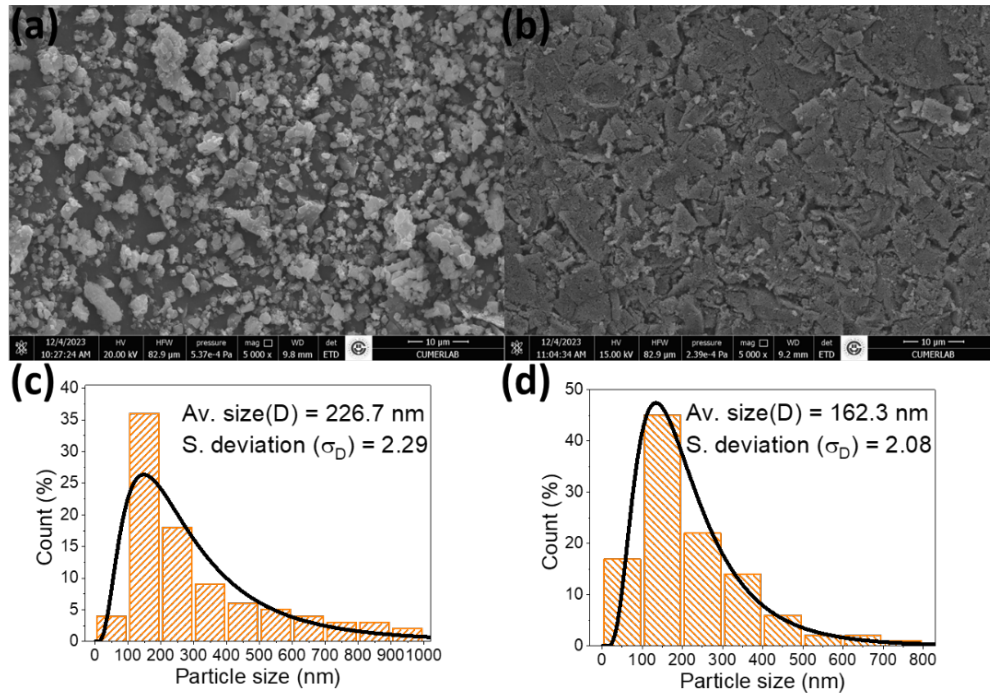


Figure 3: SEM micrographs of the LiAlO₂ samples in a) powder form, and b) pellet form; and the histogram (bars) with a log-normal function (red curve) to analyse the average size distribution for the LiAlO₂ samples in c) powder form, and d) pellet form

3.2. Luminescence Properties

Simple TL glow curves and OSL signals of LiAlO₂ pellets exposed to 1 Gy beta dose are shown in Fig. 4. The TL glow curves of LiAlO₂ pellets consist of a shoulder TL peak located at approximately 200 °C, followed by more delicate TL peak with a maximum located around 110 °C (see Fig. 4a). In the TL curves at higher temperatures, unstable signals caused by background subtraction are observed, so it is too early to talk about the existence of a significant TL trap in this region. On the other hand, the OSL decay curve of LiAlO₂ pellet exposed to 1 Gy is presented by log-log scales in Fig. 4b. After a preheating treatment at 100 °C/10 s, the obtained OSL signals exhibit two decaying parts (fast and slow), and the OSL signals come the background (zero) level in approximately 10 s. It can be said that LiAlO₂ pellets have sufficient sensitivity for personal and accident dosimetry studies that require relatively higher dose measurements.

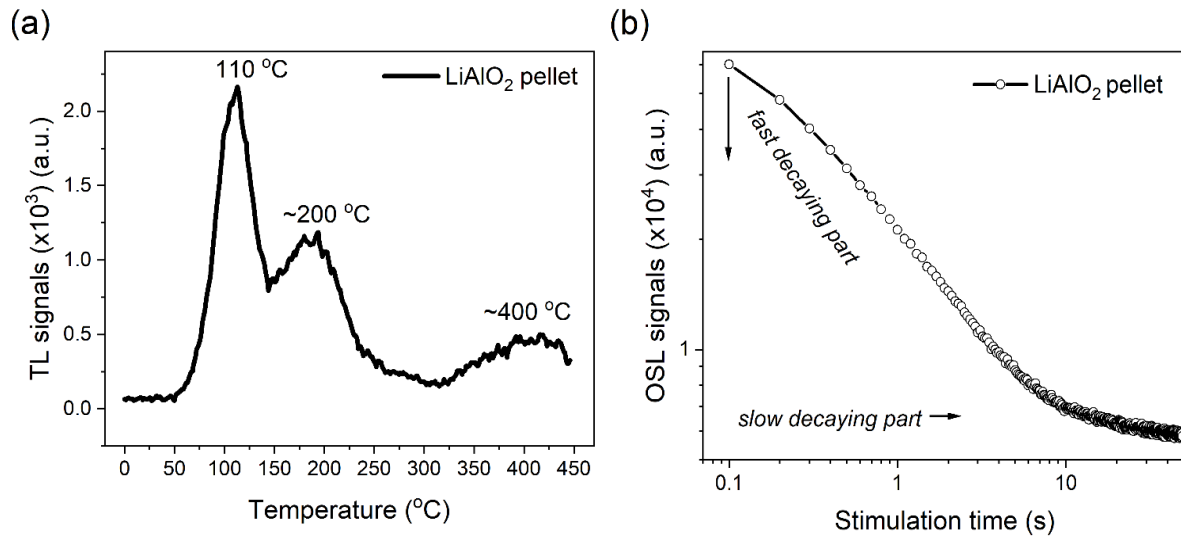


Figure 4: a) TL glow curve; b) OSL decay curve of the LiAlO₂ pellet sample. Sample was exposed to a beta dose of 1 Gy before TL and OSL readouts. Heating rate is 2 °C/s

Analysis of the OSL decay curve of LiAlO₂ is a crucial initial step to recognize the host material. Figure 5 shows the experimental OSL decay curve and their three first-order components analyzed via curve fitting. As can be seen from the figure, the OSL decay curve obtained from the LiAlO₂ pellet was well fitted to three time-decaying functions with an acceptable FOM value as 1.04. Undoubtedly, this OSL decay curve analysis method was also studied as the linear sum of two separate components, but when the fit quality was checked, the FOM value remained above 3.00. For this reason, three separate components were considered. It should be noted that this method is a simplified approach and does not provide precise information about actually existing trap levels and charge transfer.

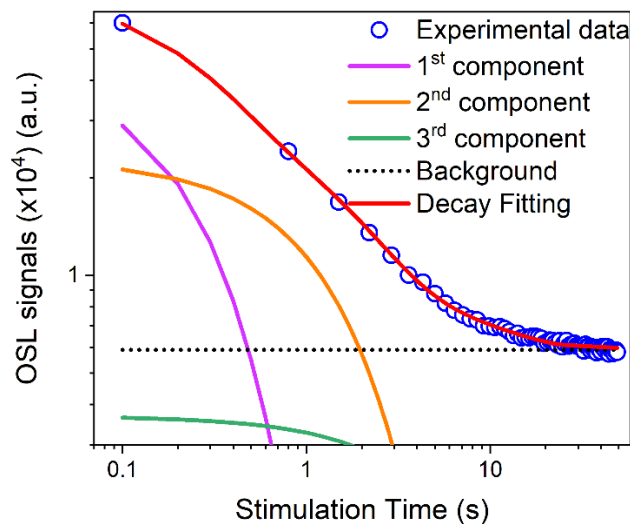


Figure 5: OSL decay curve and its components for the LiAlO₂ pellet samples which were previously irradiated with 1 Gy beta doses

RL emissions have been studied as a useful initial method providing information about the luminescence bands of dosimetric materials. Figure 6 shows the RL emission obtained from the sample during x-ray irradiation from 200 nm to 1000 nm. As can be seen from the figure, the emission of LiAlO_2 is represented by luminescence bands located in two different regions. It has a low sensitivity UV-Blue luminescence band located at 350 nm in the range from 200 to 500 nm and a broad luminescence band located at 740 nm between 600 nm and 850 nm towards the end of the visible region. There are many different speculations in the literature regarding the emission bands observed between 600 nm and 850 nm. While the emission band observed at 740 nm was attributed to the Fe^{3+} impurity unintentionally present in the Al_2O_3 used initially [28], it has also been suggested that some vacancy defects (such as large amounts of single-ion oxygen vacancies-surface disorder-oxygen interstitials-aluminium interstitials) at the deep levels of the band gap are responsible [4, 13, 29, 30].

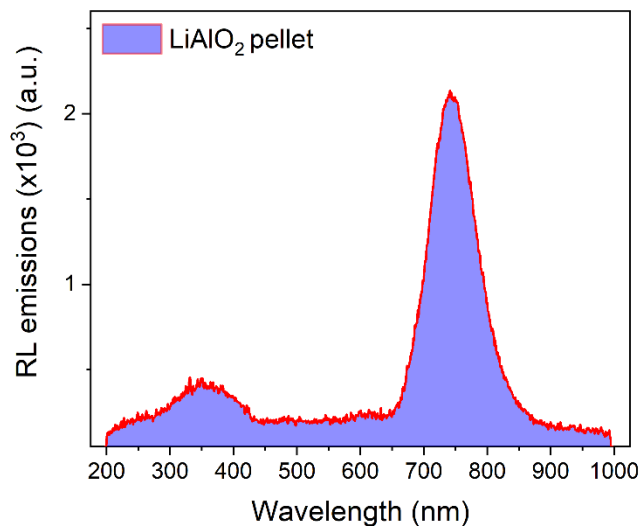


Figure 6: RL emissions of LiAlO_2 pellet

Figure 7 presents a contour plot of TL emission spectra obtained from LiAlO_2 pellet between 390 and 900 nm. As seen from the figure, a wide emission band around 740 nm dominates in TL emissions. It is seen that TL traps are close to each other and overlap between 100 °C and 300 °C. Comparing the RL and TL emissions in the range of 400 nm to 900 nm, it is found that the TL and RL emissions are almost the same. This may mean that similar recombination centres are involved in luminescence in both luminescence processes. The actual luminescence mechanism is undoubtedly much more complex. Here, with simplified approximations, it can be inferred that after the radiation dose, charge-trapped carriers in the intrinsic defects of LiAlO_2 (oxygen vacancies, surface defects, etc.) result in the emissions observed by electron/hole recombination in V-type defects.

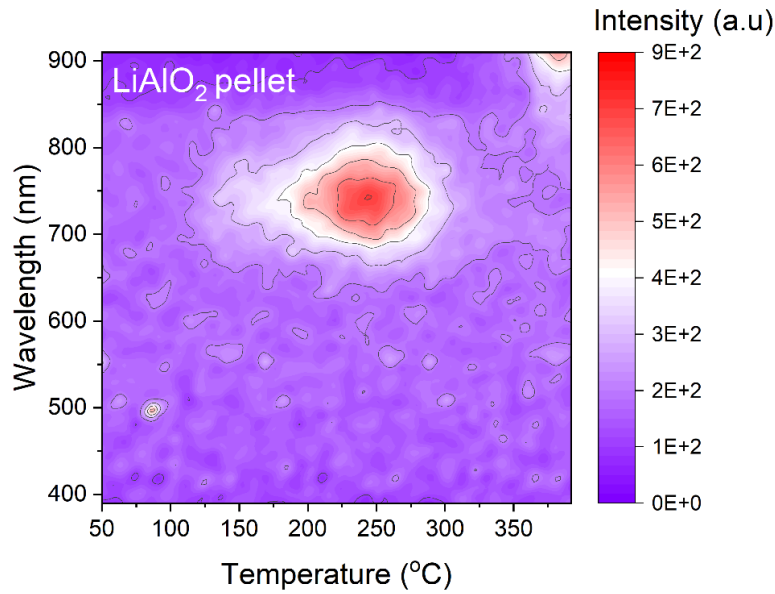


Figure 7: The colour map plot of the TL emission (390–900 nm) of LiAlO₂ pellet after 600 s excitation.

4. Conclusion

This study revealed the production, structural and morphological characterization, and luminescence properties of LiAlO₂ material, a promising host material for OSL dosimetry, using the sol-gel synthesis method. LiAlO₂ crystals were successfully synthesized by the sol-gel method in the tetragonal phase, and in SEM analysis, it was observed that the grain sizes of the powder samples decreased with the pelletization process and ceramic structures with smooth surface forms were obtained. LiAlO₂ pellets offered promising OSL response in the UV region, although their TL sensitivity was low. It was concluded that the RL and TL emission luminescence bands obtained between 400 and 900 nm were similar and they may be using the same recombination centers. LiAlO₂ is a suitable host to produce more sensitive luminescent materials in OSL dosimetry. With this study, the luminescence source of LiAlO₂-based materials was identified and it was concluded that they can be used in dose measurement in radiation measurement applications with future doping studies.

Acknowledgements

This study was supported financially by the Çukurova University Research Projects Development and Coordination Unit under contract number FKB-2023-16411. Therefore, I am grateful to the Rectorate of Çukurova University for their financial support. I thank Prof. Kasım Kurt and Özlem Yiğit from Mersin University for their valuable contributions to RL and TL emission measurements.

References

[1] Bøtter-Jensen, L., McKeever, S.W.S., Wintle, A.G., *Optically stimulated luminescence dosimetry, 1st ed*, 355 pp, Elsevier, 2003.

- [2] McKeever, S.W.S., Moscovitch, M., *On the advantages and disadvantages of optically stimulated luminescence dosimetry and thermoluminescence dosimetry*, *Radiation Protection Dosimetry*, 104(3), 263-270, 2003.
- [3] Akselrod, M.S., Bøtter-Jensen, L., McKeever, S.W.S., *Optically stimulated luminescence and its use in medical dosimetry*, *Radiation Measurements*, 41(1), 78-99, 2006.
- [4] Altunal, V., Guckan, V., Ozdemir, A., Yegingil Z., *A calcination study on BeO ceramics for radiation dosimetry*, *Materials Research Bulletin*, 130, 110921, 2020.
- [5] Ozdemir, A., Altunal, V., Guckan, V., Kurt, K., Yegingil Z., *Luminescence characteristics of newly-developed $MgB_4O_7:Ce^{3+},Na^+$ phosphor as an OSL dosimeter*, *Journal of Alloys and Compounds*, 865, 158498, 2021.
- [6] Altunal, V., Ozdemir, A., Kurt, K., Yigit, O., Guckan, V., Isik, B., Yegingil Z., *Luminescence properties of Ce and Be-doped $CaAl_{12}O_{19}$ for dosimetric and light-emitting applications*, *Journal of Alloys and Compounds*, 985, 174081, 2024.
- [7] Guckan, V., Altunal, V., Ozdemir, A., Yegingil Z., *Optically stimulated luminescence of $MgO:Na,Li$ phosphor prepared using solution combustion method*, *Journal of Alloys and Compounds*, 835, 155253, 2020.
- [8] Ozdemir, A., Guckan, V., Altunal, V., Kurt, K., Yegingil Z., *Thermoluminescence in $MgB_4O_7:Pr,Dy$ dosimetry powder synthesized by solution combustion synthesis method*, *Journal of Luminescence*, 230, 117761, 2021.
- [9] Nur, N., Guckan, V., Kizilkaya, N., Depci, T., Ahmedova, C., Ozdemir, A., Altunal, V., Yegingil Z., *Thermoluminescence properties of non-stoichiometric $Li_2Si_2O_5$ synthesized from natural amethyst quartz*, *Journal of Luminescence*, 179, 366-371, 2016.
- [10] McKeever, S.W.S., Akselrod, M.S., Colyott, L.E., Agersnap Larsen, N., Polf, J.C., Whitley, V., *Characterisation of Al_2O_3 for use in thermally and optically stimulated luminescence dosimetry*, *Radiation Protection Dosimetry*, 84(1-4), 163-166, 1999.
- [11] Akselrod, M.S., Lucas, A.C., Polf, J.C., McKeever, S.W.S., *Optically stimulated luminescence of Al_2O_3* , *Radiation Measurements*, 29(3-4), 391-399, 1998.
- [12] Dhabekar, B., Raja, E.A., Menon, S., Gundu Rao, T.K., Kher, R.K., Bhatt,nB.C., *Identification of defect centres using TSL, PL, OSL and ESR studies in $LiAlO_2$ based phosphors*, *Journal of Physics D: Applied Physics.*, 41, 115414, 2008.
- [13] Jopat, P.R., Sisodiya, D.S., Sen, S., M.S. Kulkarni, *$LiAlO_2:Sm$ a highly sensitive and multi-functional radiation dosimeter*, *Ceramics International*, 48(24), 36593-36600, 2022.
- [14] Wani, M.A., Dhoble, S.J., Belekar, R.M., *Synthesis, characterization and spectroscopic properties of some rare earth activated $LiAlO_2$ phosphor*, *Optik*, 226(1), 165938, 2021.
- [15] Bajaj, N.S., Omanwar, S.K., *LEDs phosphor $BaAl_2O_4:Sm$ prepared by solution combustion synthesis*, *AIP Conference Proceedings*, 1536(1), 803-804, 2013.
- [16] Poort, S., Blokpoel, W.P., Blasse, G., *Luminescence of Eu^{2+} in barium and strontium aluminate and gallate*, *Chemistry of Materials*, 7(8), 1547-1551, 1995.
- [17] Agarwal, M., Garg, S.K., Asokan, K., Kumar, P., *Temperature-dependent OSL properties of nano-phosphors $LiAlO_2:C$ and $\alpha-Al_2O_3:C$* , *Applied Surface Science*, 444, 819-828, 2018.
- [18] Lee, J.I., Pradhan, A.S., Kim, J.L., Chang, I., Kim, B.H., Chung, K.S., *Characteristics of $LiAlO_2$ -Radioluminescence and optically stimulated luminescence*, *Radiation Measurement.*, 56, 217-222, 2013.
- [19] Dickens, P.T., Marcial, J., McCloy, J., McDonald, B.S., Lynn, K.G., *Spectroscopic and neutron detection properties of rare earth and titanium doped $LiAlO_2$ single crystals*, *Journal of Luminescence*, 190, 242-248, 2017.

- [20] Takebuchi, Y., Watanabe, K., Nakauchi, D., Fukushima, H., Kato, T., Kawaguchi, N., Yanagida, T., *Scintillation properties of Ce-doped LiAlO₂ for neutron detection*, Journal of the Ceramic Society of Japan, 129(7), 397-401, 2021.
- [21] Twardak, A., Bilski, P., Marczevska, B., Lee, J.I., Kim, J.L., Gieszczyk, W., Mrozik, Sąd, A., M., Wróbel, D., *Properties of lithium aluminate for application as an OSL dosimeter*, Radiation Physics and Chemistry, 104, 76-79, 2014.
- [22] Klug, H.P., Alexander, L.E., *X-ray diffraction procedures: for polycrystalline and amorphous materials*, *X-Ray Diffraction Procedures: For Polycrystalline and Amorphous Materials*, 2nd ed, 992 pp, Wiley, 1974.
- [23] Norazlina, M.S., Shanmugan, S., Mutharasu, D., *Structural Analysis of BeO Nanoparticles Synthesized by Polyacrylamide Gel Route*, Advanced Science Focus, 1, 362-366, 2013.
- [24] Theivasanthi, T., Alagar, M., *Electrolytic synthesis and characterizations of silver nanopowder*, Nano Biomedicine and Engineering, 4(2), 58-65, 2012.
- [25] Altunal, V., Yegingil, Z., Tuken, T., Depci, T., Ozdemir, A., Guckan, V., Nur, N., Kurt, K., Bulur, E., *Optically stimulated luminescence characteristics of BeO nanoparticles synthesized by sol-gel method*, Radiation Measurements, 118, 54-66, 2018.
- [26] Altunal, V., Guckan, V., Ozdemir, A., Zydhachevskyy, Y., Lawrence, Y., Yu, Y., Yegingil, Z., *Three newly developed BeO-based OSL dosimeters*, Journal of Luminescence, 241, 118528, 2022.
- [27] Balian, H.G., Eddy, N.W., *Figure-of-merit (FOM), an improved criterion over the normalized chi-squared test for assessing goodness-of-fit of gamma-ray spectral peaks*, Nuclear Instruments and Methods, 145, 389-395, 1977.
- [28] Pejchal, J., Fujimoto, Y., Chani, V., Yanagida, T., Yokota, Y., Yoshikawa, A., Nikl, M., Beitlerova, A., *Modifications of micro-pulling-down method for the growth of selected Li-containing crystals for neutron scintillator and VUV scintillation crystals*, Journal of Crystal Growth, 360, 127-130, 2012.
- [29] Li, P.G., Lei, M., Tang, W.H., *Raman and photoluminescence properties of α -Al₂O₃ microcones with hierarchical and repetitive superstructure*, Materials Letters, 64(2), 161-163, 2010.
- [30] Tavernier, S., Gektin, A., Grinyov, B., Moses, W.W., *Radiation detectors for medical applications*, 1st ed, 307 pp, Springer Dordrecht, 2006.